MASSACHUSETTS INSTITUTE OF TECHNOLOGY
LINCOLN LABORATORY

MILLSTONE HILL THOMSON SCATTER RESULTS FOR 1967

J. V. EVANS

Group 21

TECHNICAL REPORT 482

22 JULY 1971

LEXINGTON AIR FORCE 37360 14 January - 400 MASSACHUSETT

The work reported in this document was performed at Lincoln Laboratory, a center for research operated by Massachusetts Institute of Technology. The work is sponsored by the Office of the Chief of Research and Development, Department of the Army; it is supported by the Advanced Ballistic Missile Defense Agency under Air Force Contract F19628-70-C-0230.

ABSTRACT

This report summarizes results for the electron density distribution and electron temperature of the F-region obtained during 1967 using the Millstone Hill (42.6°N, 71.5°W) Thomson (incoherent) scatter radar system. These data, for the height interval of approximately 200 to 800 km, were gathered over 24-hour observing periods twice per calendar month. The time required to obtain a complete electron density and temperature profile over this height interval was 30 minutes.

The results show a far wider range of behavior than that encountered in previous years. This is attributed to the increase in magnetic activity as sunspot maximum is approached. On magnetically quiet days, the characteristic behavior observed previously for electron density manifests itself. Winter days exhibit a maximum at all levels near noon and a weaker maximum at the layer peak in the early morning (0200 to 0400 EST), while summer days exhibit a maximum near sunset and only a small day-to-night change in density near the layer peak. Two days exhibited a pattern of behavior, first noted in 1965, that appears characteristic of many storms. This consists of an increase in density on the afternoon of the first day of the storm followed by a marked decrease the next morning. Other days show instances of nocturnal heating and erratic behavior of the F-region electron density at night. We believe that on several occasions in 1967 the plasmapause boundary moved south of Millstone giving rise to a rapid fall in f_oF2 and to much of the irregular behavior observed at night.

Accepted for the Air Force
Joseph R. Waterman, Lt. Col., USAF
Chief, Lincoln Laboratory Project Office

CONTENTS

MILLSTONE HILL THOMSON SCATTER RESULTS FOR 1967

I. INTRODUCTION

Thomson (incoherent) scatter radar measurements of F-region electron densities and temperatures were made at Millstone Hill, Westford, Massachusetts (42.6°N, 71.5°W), approximately twice per month throughout 1967 for periods usually of 24 hours. This report summarizes the results obtained and discusses these in relation to the behavior observed in previous years (Table I). Earlier reports in this series[1-4] present the results of synoptic studies carried out in the years 1963 through 1966. Results obtained during some of the months in these years are discussed in greater detail in a number of journal articles as referenced in Table I.

TABLE I

PUBLICATIONS CONCERNING THE MILLSTONE HILL UHF (68-cm Wavelength) THOMSON SCATTER RESULTS

Year	Months Covered	Publication
1963	February 1963 to January 1964	Ref. 1
	March, July, August, September	Ref. 5
	April, July, November	Ref. 6
1964	January through December	Ref. 2
	April, July, November	Ref. 7
1965	January through December	Ref. 3
	June, August, September	Refs. 8, 9
	June	Ref. 10
	January, April, July	Ref. 11
1966	January through December	Ref. 4

Section II provides a summary of the equipment, observing and data-processing procedures employed during 1967. These differed little from those of the latter half of 1965 which are fully documented in Ref. 3. In Sec. III, the results obtained for electron density are discussed. Section IV presents electron temperature results along with average daytime and nighttime electron temperature profiles obtained for each 24-hour period. These averages are employed, in Sec. V,

to derive seasonal temperature variations and seasonal variations in the heat conducted into the F-region from the magnetosphere. Section VI provides a summary of the results.

II. EQUIPMENT, OBSERVING AND DATA PROCESSING PROCEDURES

A. Equipment

The UHF incoherent scatter radar equipment has been described previously.[1] No major alterations were made in 1967, though the first of a series of changes to the antenna were made. These were designed to reduce the problem of ground-clutter returns. Echoes are observable out to a range of ~160 km and make it difficult or impossible to obtain useful results at or below about 200 km* using the vertically directed UHF radar system. A study of the antenna indicated that the chief source of these echoes is radiation scattered off the legs of the tripod supporting the antenna feed horn. To reduce these reflections, absorbing netting was placed on the inside of the legs a quarter of a wavelength away. In addition, a conical skirt was built and placed around the horn to lower the intensity of the radiation emerging at large angles to its axis. These measures reduced the intensity of the ground-clutter echoes sufficiently that, as a rule, they no longer saturated the receiver. This in turn permitted the duration of the receiver suppression to be shortened, so that it became possible to extend the electron density profile measurements to lower altitudes than heretofore. However, clutter-free records were not obtained until 1970 when digital filtering procedures were developed that remove ground-clutter echoes from the data.

Another series of improvements initiated in 1967 was the replacement of the old vacuum-tube portions of the receiver by solid-state components. Most important of these changes was the substitution of a regenerative-diode parametric amplifier for the electron-beam-tube parametric amplifier (Adler tube) employed previously. Earlier attempts to employ solid-state parametric amplifiers had always run into difficulties caused by transient voltages, appearing across the TR switch cavity, which burned out the diodes. With the development of solid-state limiter circuits this problem has been eliminated.

The electron-beam parametric amplifier employed prior to 1967 was operated with a synchronous pump frequency at 880 MHz. This caused the image and signal channels to be superimposed. That is, the device operated simultaneously as an amplifier and as a sideband inverter so that both sidebands were made the same. The advantage of this was that the noise temperature of the image channel could be minimized by ensuring a good match to the antenna terminals. However, because the sidebands are inverted, the phase information in the signal is lost. This means that any shift in the spectrum due to drifts in the ionosphere cannot be detected. Further, because samples of the signal have only a single degree of freedom, the uncertainty in the estimate of the received power P_s after N samples is $\pm\sqrt{2}\ P_s/\sqrt{N}$ in place of $\pm P_s/\sqrt{N}$ for a conventional amplifier. Stated otherwise, in the case of weak signals, the effective noise temperature is 1.4 times the measured system temperature. The new parametric amplifier obviated both problems but was not without its own drawbacks. One of these was large gain variations with changes of ambient temperature. Later, in 1969, it became necessary to put additional thermal insulation inside the hut (under the antenna) that houses the first stages of the receiver, in order to reduce this effect to a manageable level.

---

* Some measurements in the altitude range 120 to 240 km have been obtained at Millstone Hill using a smaller 84-foot-diameter L-band radar at oblique incidence.[12-14]

B. Observing Procedures

The observing procedures were changed in 1965 to reduce the amount of time required to obtain a complete electron density and temperature profile from 1 hour to 30 minutes. This was accomplished by recording the IF signals for later non-real-time processing. The recording and playback system, discussed extensively in Ref. 3, was employed throughout 1967.

In addition to this change, the spectrum analyzer was modified in June 1965 to permit both halves of the signal spectrum to be explored. Unfortunately, this was carried out in a way which, though not recognized at the time, caused some loss of information. As a result, the values obtained for ion temperature are unreliable between about 300 and 500 km and therefore are not included in this report. These changes and means of minimizing the unwanted effects they introduced in the results are discussed in Ref. 3 and will not be repeated here.

During 1967 we attempted to make observations twice per month for a period of 24 hours. Table II lists the dates and times on which measurements were carried out together with the mean of the planetary magnetic index Kp over the period of observation. Equipment malfunctions caused the loss of some data; and we have been obliged to combine measurements made on 24-25 February with others on 2 March to obtain a complete 24-hour period.

In addition to the 24-hour observations discussed here, measurements were made for a number of 12-hour periods in January, February and March to examine the behavior of the electron temperature at conjugate sunrise. These measurements have already been reported[15] and will not be included here.

C. Data Reduction

Data reduction procedures for measurements in 1967 were the same as those employed for 1966 and are compared with those of earlier years in Table III. Basically each set of observations was reduced to obtain an electron density profile and electron and ion temperature curves, which were then employed to obtain contours of these parameters vs height and time.

One advance made during the year was the automation of part of the work needed to produce the electron density profile. Previously, the computer was employed to draw "Calcomp" plots of the power profile (i.e., the echo power times the square of the height) observed with each of the three pulse lengths employed (0.1, 0.5 and 1.0 msec). These plots were then superimposed and converted into a single curve that combined the good height resolution afforded by the short pulse measurements (at low altitudes) with the greater accuracy achieved using long pulses at heights above $h_{max}F2$ where the signal-to-noise ratio becomes poor. This combined curve was then corrected for the variation of the electron-to-ion temperature ratio T_e/T_i with altitude. In place of this time-consuming hand operation, a computer program was developed to combine the profiles and plot the resulting curve. This program employed the short pulse (0.1-msec results) up to some fixed altitude (400 km) and then fitted to these the long pulse results in straight line sections on a log plot. These straight line sections covered 50-km height intervals and were obtained by fitting least-mean-square straight lines to the logarithms of the data points. In deciding when to discontinue using the 0.5-msec results and transfer to the 1.0-msec curve, we made use of the fact that the scale height of the ionization $[k(T_e + T_i)/m_i g]$ should increase monotonically with altitude. Thus, in fitting these lines, the 0.5-msec results were used above 400 km until a 50-km height interval was encountered in which the slope of the line was found to be lower than the previous one. (That such an interval is encountered is an inevitable consequence of the

TABLE II

INCOHERENT SCATTER OBSERVATIONS – 1967

Begin			End			Mean	Comment
Date	C*	EST	Date	C*	EST	Kp†	
5 January	q	1100	6 January		1200	1+	Quiet – data prior to 1900 lost
24 January	Q	0030	25 January		1200	1+	Quiet – most temperature data lost
6 February		1200	7 February	D	1200	2_o	
24 February	Q	1800	25 February	D	0100	2+	Combined
2 March	Q	0030	2 March		1800	1+	
13 March		1400	14 March		1130	1+	Quiet
27 March	D	1200	28 March		1100	3–	Somewhat disturbed
6 April		1130	7 April		1130	2_o	
24 April	D	1200	25 April		2300	2_o	
11 May		1030	12 May		1030	3_o	Disturbed
22 May		1200	23 May		1100	1_o	Quiet
8 June	Q	1100	9 June		1000	3_o	Disturbed
22 June	q	1100	23 June	Q	1030	1–	Quiet
5 July	D	1100	6 July		1100	2–	
25 July		0830	26 July		0930	2_o	
15 August		1030	16 August	q	1100	1+	Quiet
29 August		1100	30 August		1200	2_o	
12 September		1100	13 September	q	1200	1+	Quiet
28 September	q	1300	29 September		1200	2–	Disturbed
10 October	Q	1230	11 October	Q	1030	1–	Quiet
24 October		1100	25 October		1030	1+	Quiet
7 November	Q	1200	8 November	D	1100	2+	Somewhat disturbed
21 November	q	1100	22 November		1100	3–	Somewhat disturbed
5 December		1200	6 December		1200	4–	Disturbed
19 December	D	1230	20 December	D	1200	5–	Very disturbed

* Condition:

Q One of five quietest days in month
q One of ten quietest days in month
D One of five most disturbed days in month

† Planetary magnetic index.

TABLE III

OBSERVING PROGRAM AS A FUNCTION OF YEAR

Year	Length of Each Observing Period (hours)	Number of Observing Periods per Month	Time Taken to Measure One Profile (hours)	Number of Profiles Obtained per Month	Reduction Method Employed
1963	30	4	1.5	80	Mean hourly profiles constructed for each calendar month
1964	30	2	1.0	60	As above
1965	48	1	0.5	96	As above
1966	24	2	0.5	96	Each profile analyzed separately
1967	24	2	0.5	96	As above

fact that the uncertainty and hence the scatter of the points increases rapidly with altitude.) At this point the 1.0-msec results were employed in place of the 0.5-msec measurements and the process was continued until these too yielded a decrease in scale height with altitude.

This procedure did not obviate the need to correct the power profiles for the altitude variation of the electron-to-ion temperature ratio (T_e/T_i) and this was carried out by hand.* In this and all other respects the data processing procedures employed in 1966 were the same as those discussed previously for 1965 (Ref. 3). Figure 1 shows an example of one of these machine drawn plots together with the true density profile after applying a correction for the variation of T_e/T_i with altitude.

III. ELECTRON DENSITY RESULTS

A. Electron Density Profiles

The combined density profiles were assigned an absolute scale by adjusting the peak density N_{max} so that

$$N_{max} = 1.24\,(f_oF2)^2 \times 10^4\ cm^{-3} \tag{1}$$

where f_oF2 is the critical frequency of the F2 layer (MHz). To obtain f_oF2, the available values for the stations at Millstone, Billerica, Fort Belvoir and Wallops Island were plotted and a smooth curve drawn through the points in such a way that it followed the Millstone and Billerica points as far as possible.[4] In some instances, no values were available for either of these stations. These cases appear to have occurred chiefly on magnetically disturbed nights when f_oF2 fell to extremely low values. In these cases we have been obliged to construct the variation of f_oF2 from the variation of the observed echo power with time. To do this, the calibration constant K was obtained for the radar results via

$$K = \frac{(T_s h^2)_{max}}{N_{max}} \tag{2}$$

* Complete machine processing of these data became possible in 1968 following the construction of a new spectrum analyzer (Ref. 16).

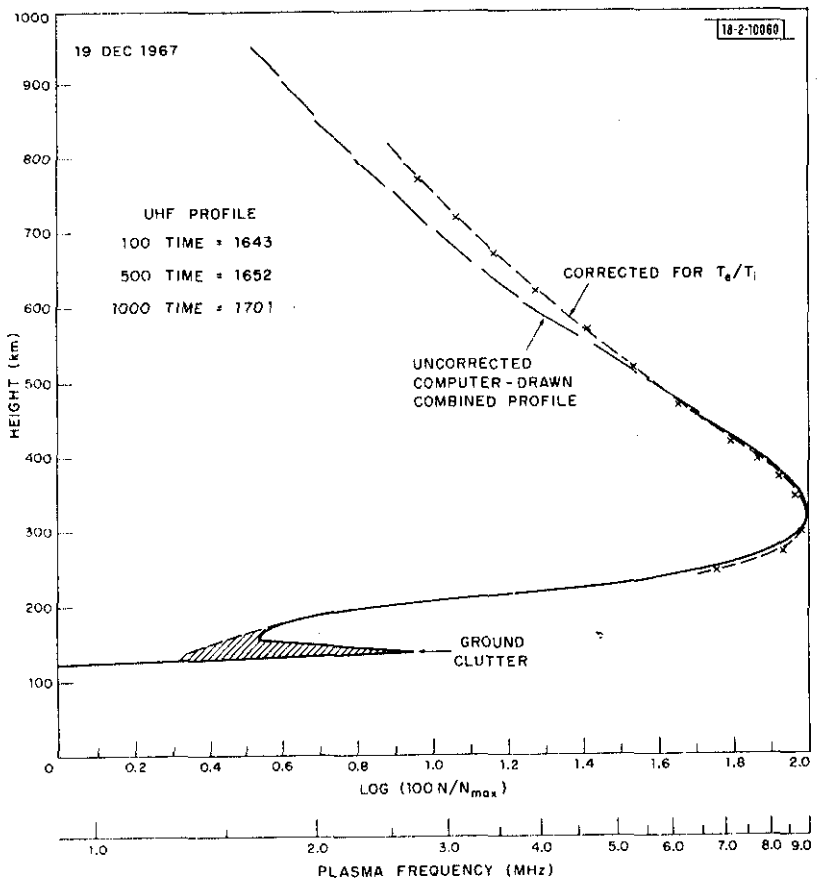

Fig. 1. Computer-drawn profile of electron density vs altitude, combining measurements made with pulses of 100, 500 and 1000 μsec commencing at the times shown. The spike near 140 km altitude is a ground-clutter echo and the receiver was suppressed out to 125 km altitude. The second curve shows the final density profile after correcting for the variation with altitude of the electron to ion temperature ratio T_e/T_i.

where T_s is the equivalent echo temperature and h the corresponding altitude. A mean of several values of K was obtained from measurements taken both prior to and following the period for which f_oF2 was missing. Figure 2(a) provides an example of a curve of f_oF2 completed in this manner for 28 September. The extremely rapid fall in f_oF2 observed at Millstone on this occasion was not seen at Fort Belvoir or Wallops Island. Similar behavior was encountered on 10-11 October, 5-6 December and 19-20 December. The behavior on this last day is particularly striking since f_oF2 fell from 9.5 to 1.5 MHz in about an hour [Fig. 2(b)]. We believe that these were all occasions on which the boundary between the midlatitude ionosphere and the trough region of low F-region ionization[17] moved south past Millstone. This phenomenon has not previously been observed at Millstone.

During several observing periods in the latter half of 1967, peculiar electron density profiles were seen at night. In some instances, e.g., 28-29 September the profiles appeared reasonably normal up to ~450-km altitude and then departed from the expected curve in a violent fashion as shown in Fig. 3. In these instances there was little similarity in the behavior observed above 400 km from run-to-run. We are inclined to attribute this behavior to the detection of weak auroral returns seen obliquely at great ranges in the sidelobes of the antenna.

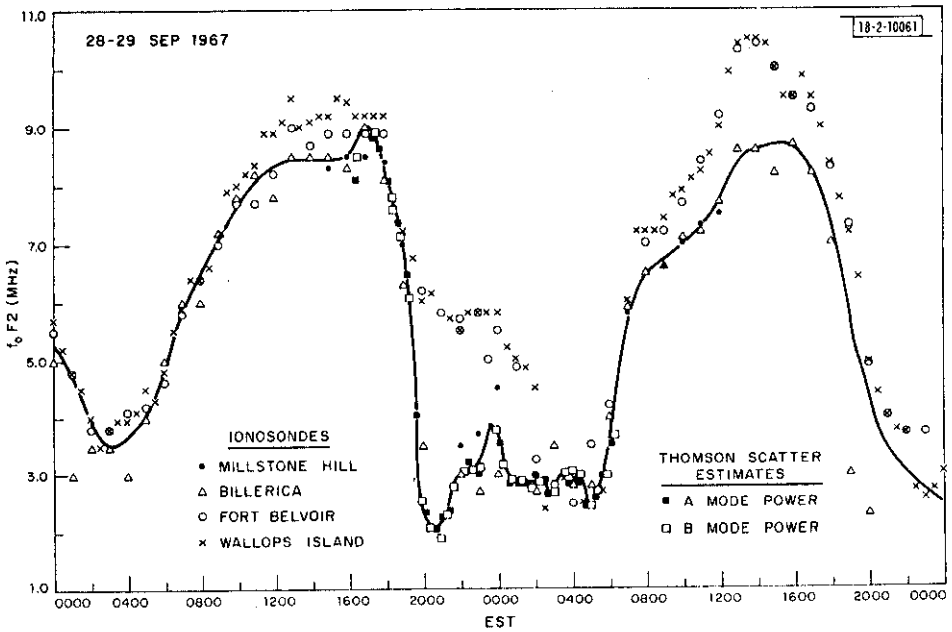

Fig. 2(a). Variation of f_oF2 on 28-29 September. In this instance, values for the period 1900 to 0600 were constructed from the variation of the total echo power [Eq. (2)], since the ionosondes at Millstone and Billerica gave few reliable values.

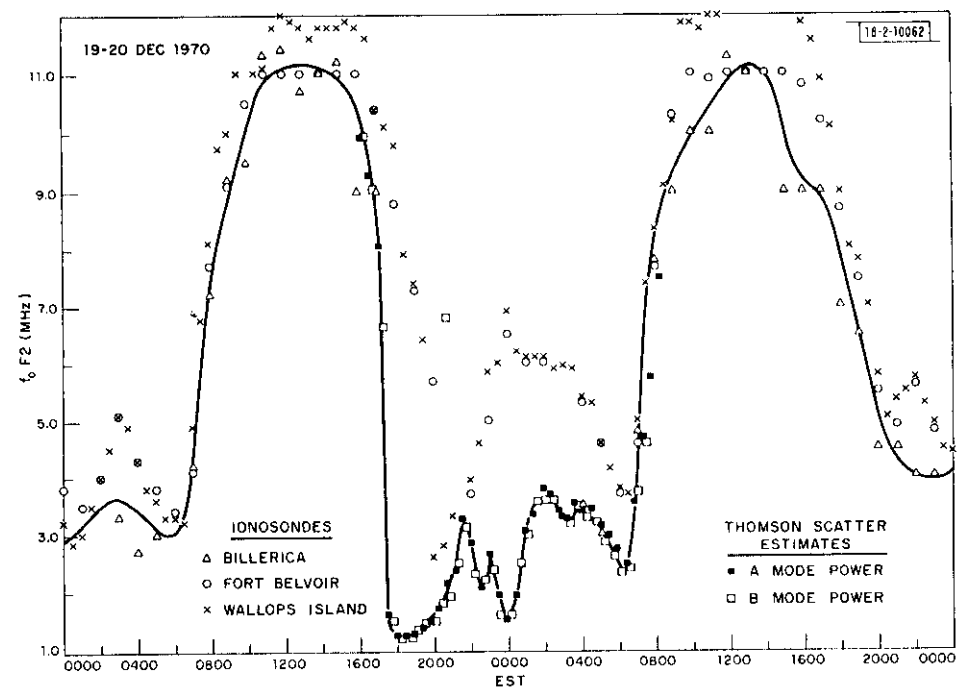

Fig. 2(b). Variation of f_oF2 on 19-20 December showing the extremely rapid fall near 1700 deduced from the variation of total echo power.

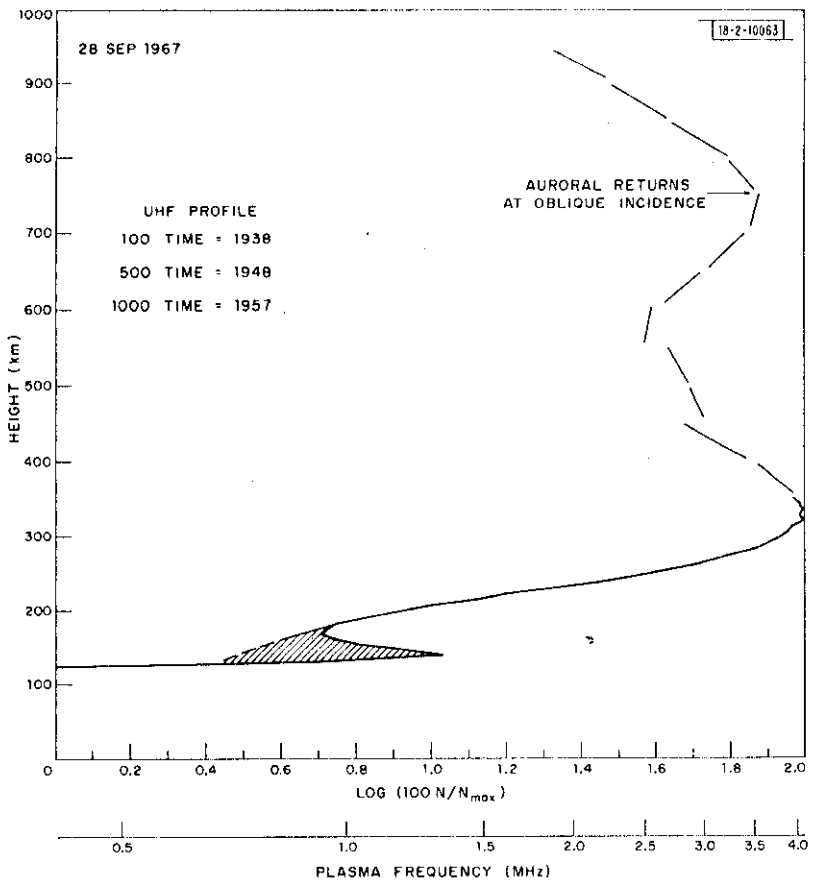

Fig. 3. Strange electron density profile observed on 28 September near 1940 EST in which there is a second F-layer peak. We believe that this second peak is spurious and arises from weak auroral returns in the sidelobes of the vertically directed antenna. [Times are for the commencement of runs with the different pulse lengths (μsec) and are in EST.]

Figures 4(a) and (b) illustrate a different form of peculiar behavior. Here an additional layer appears to be present beneath the normal F-layer. This additional layer appears to have a well defined upper edge usually near 250 km. Table IV summarizes the dates and times when the behavior illustrated in Figs. 4(a) and (b) occurred. In three cases the layer made its appearance when f_0F2 fell to a low value and disappeared at sunrise when f_0F2 began to increase. On 7-8 November the layer appeared only briefly and f_0F2 was quite high. All four nights were quite disturbed (Table II) and thus it is tempting to attribute this behavior to auroral precipitation occurring directly over Millstone. However, the very rapid fall in density near 250 km [Figs. 4(a) and (b)] is not consistent with this explanation. Further, although the height resolution achieved with 0.5-msec pulses is distinctly poorer than with 100-μsec pulses, this "layer" does not appear to have been seen using the longer pulse. This suggests that some form of equipment malfunction was occurring during the 100-μsec pulse measurements that was only clearly evident when the ionospheric echoes were extremely weak. Accordingly, we have excluded these portions of the profile from the contour diagrams presented, and have labelled these heights and times "spurious results." The exact nature of the equipment malfunction is not known.

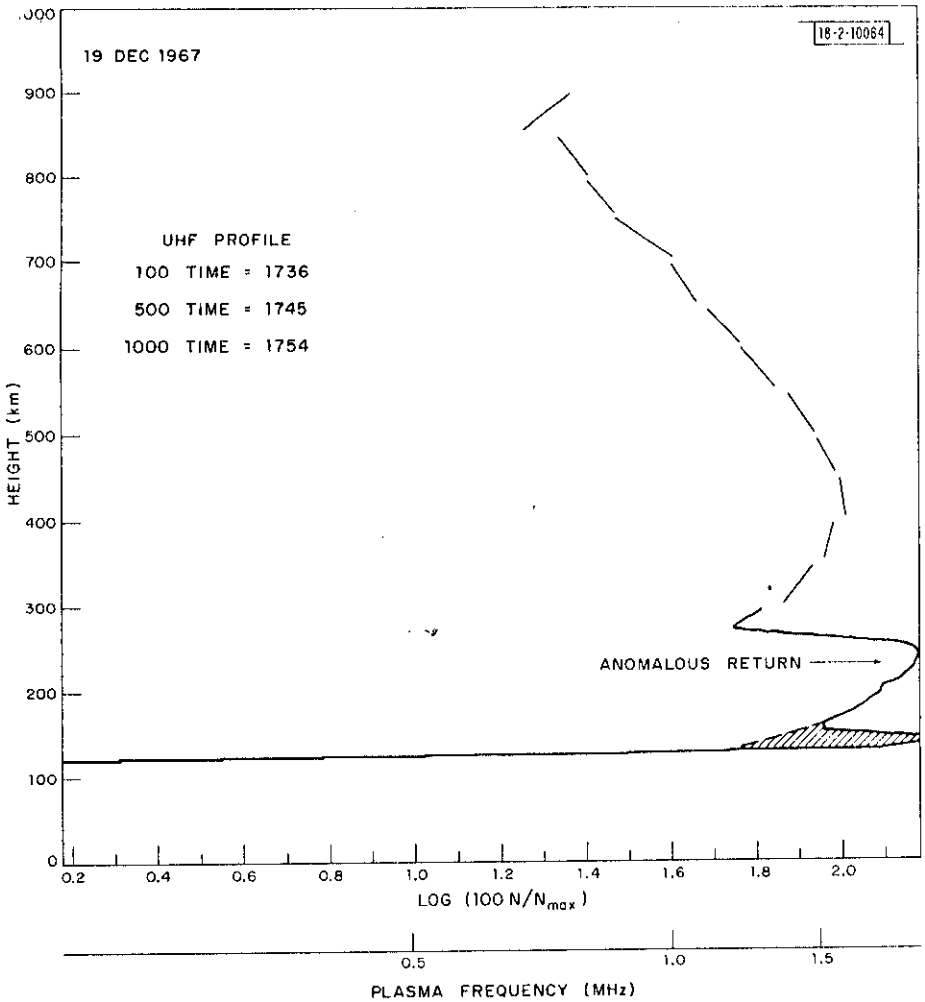

(a) 1736 to 1754 EST.

Fig. 4. Echo power profiles observed on 19-20 December that exhibit the appearance of an anomalous layer beneath the F-layer which disappeared at sunrise. We believe that this is a spurious result caused by an equipment malfunction of undertermined origin and have excluded these data from the contour diagrams.

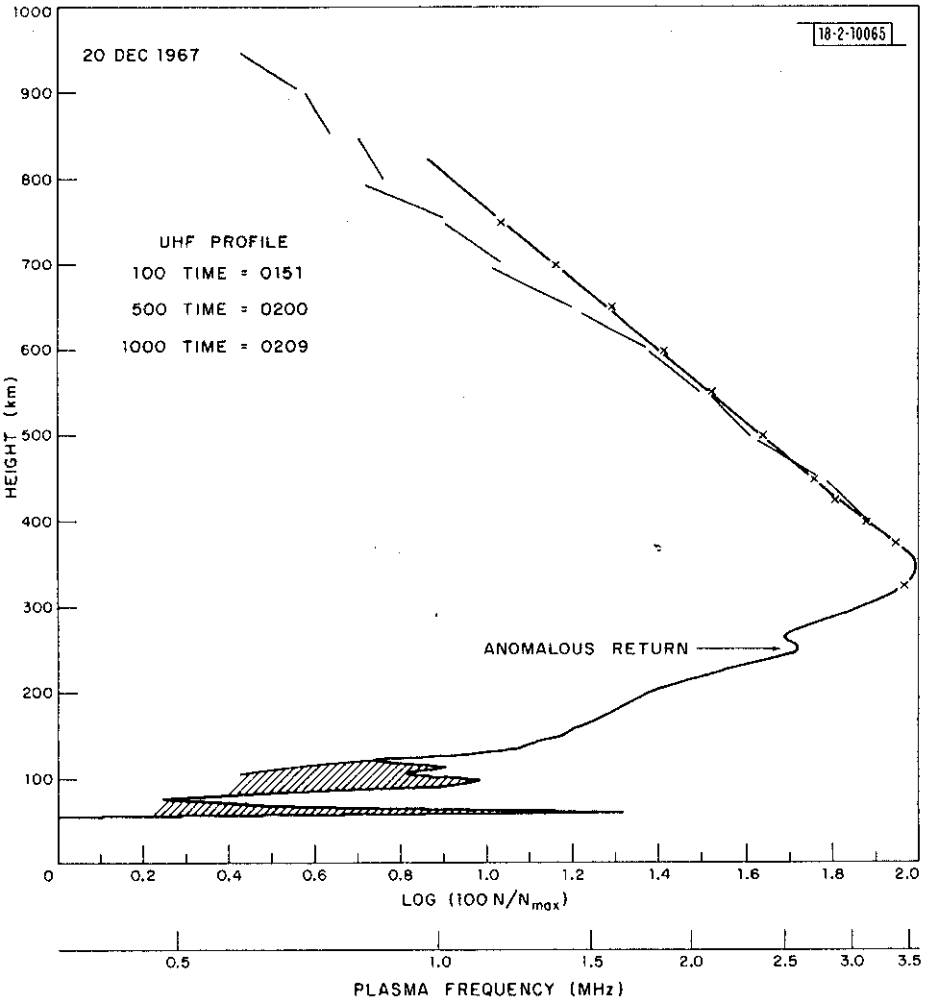

(b) 0151 to 0209 EST.

Fig. 4. Continued.

TABLE IV

CASES OF PECULIAR RESULTS AS SHOWN IN FIGS. 4(a) AND (b)

Date (1967)	Appearance		Disappearance		Height of Maximum of Lower Layer (km)
	EST	f_oF2 (MHz)	EST	f_oF2 (MHz)	
7-8 November	1902	5.8	2317	5.4	265
21-22 November	0311	3.4	0618	3.9	265
5-6 December	2321	3.2	0245	3.5	245
	0453	3.2	0644	3.3	245
19-20 December	1805	1.3	0151	3.6	250
	0339	3.3	0654	3.7	250

B. Electron Density Contour Diagrams

Figures 5(a) through (x) present contour diagrams of electron density vs height and time for the days listed in Table II. Table V summarizes the main features of these diagrams. *It is not* possible to discuss each day's measurements at length, and in what follows we select a few days to illustrate *various types of* behavior that appear to be common.

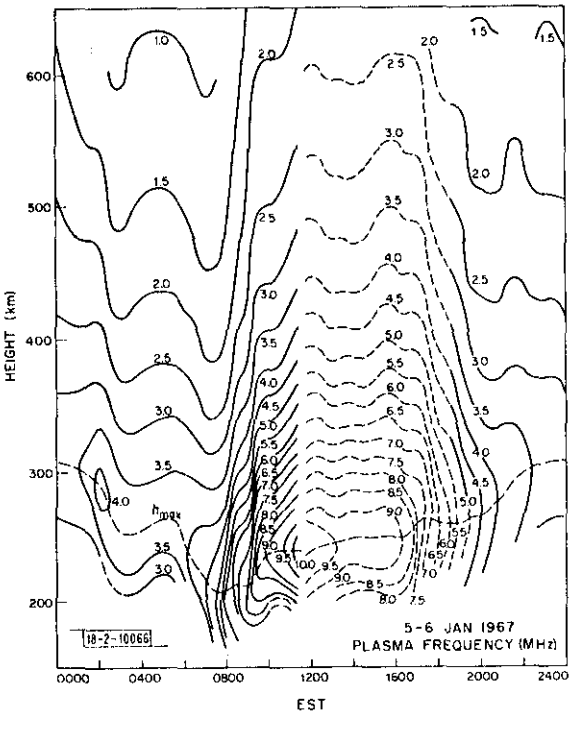

(a)

Fig. 5(a-x). Contour diagrams of constant electron density (plasma frequency) as a function of height and time for each of the observing periods.

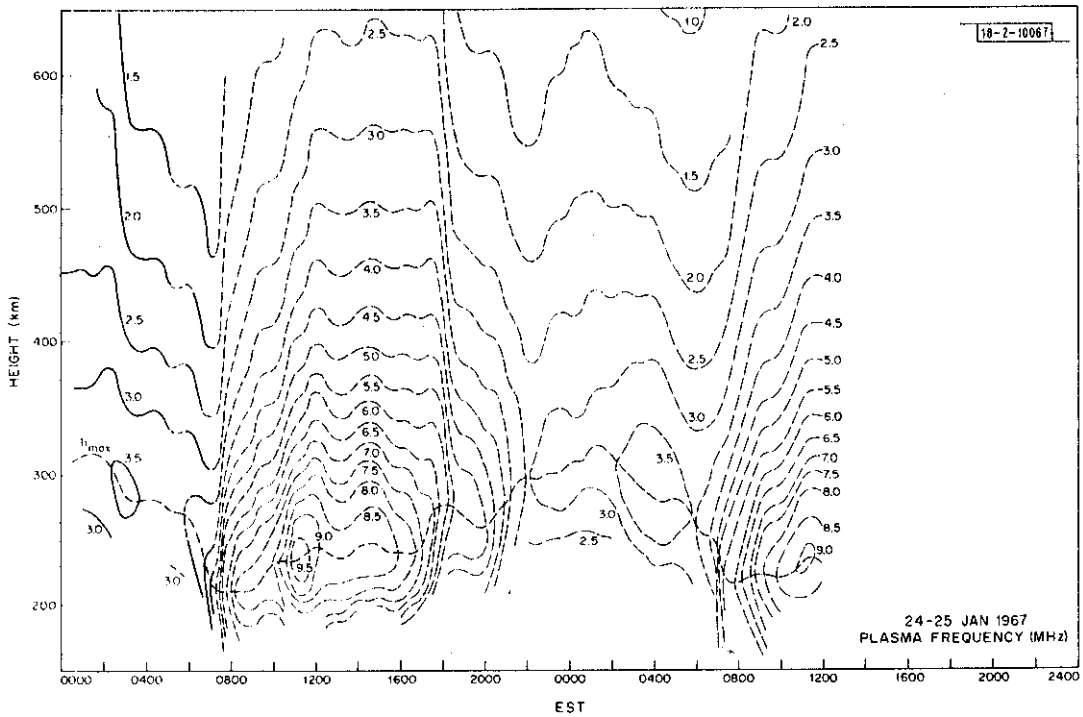

(b)

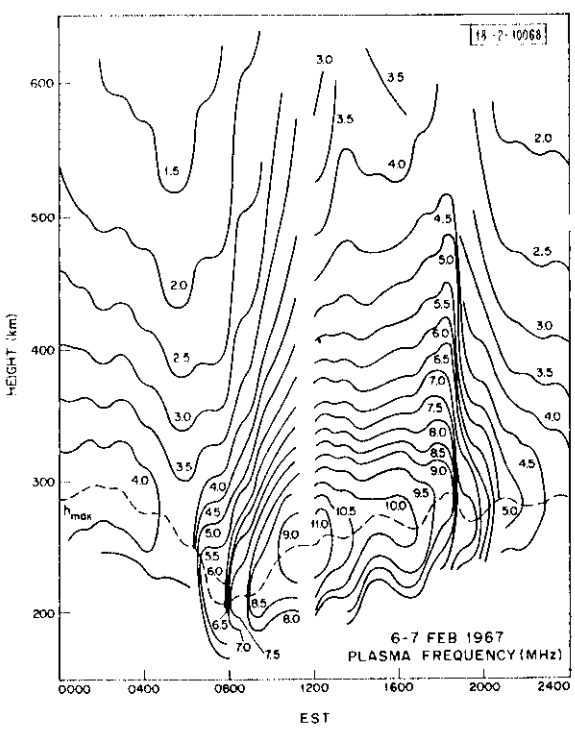

(c)

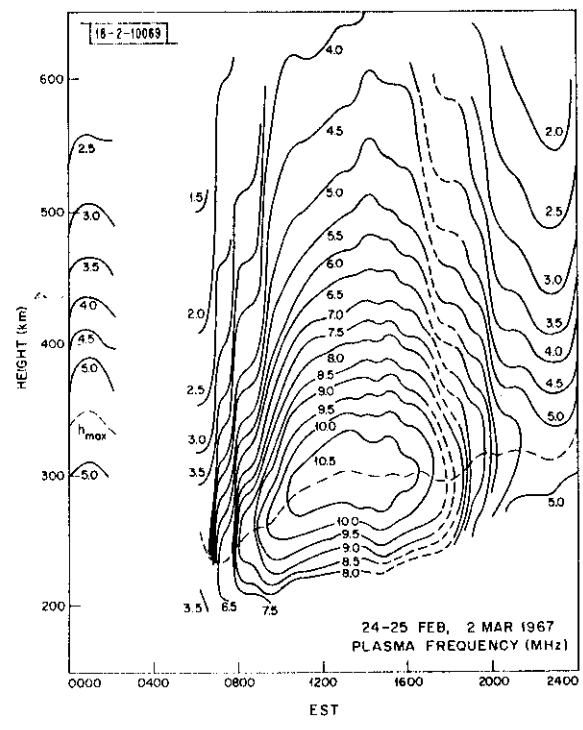

(d)

Fig. 5(a-x). Continued.

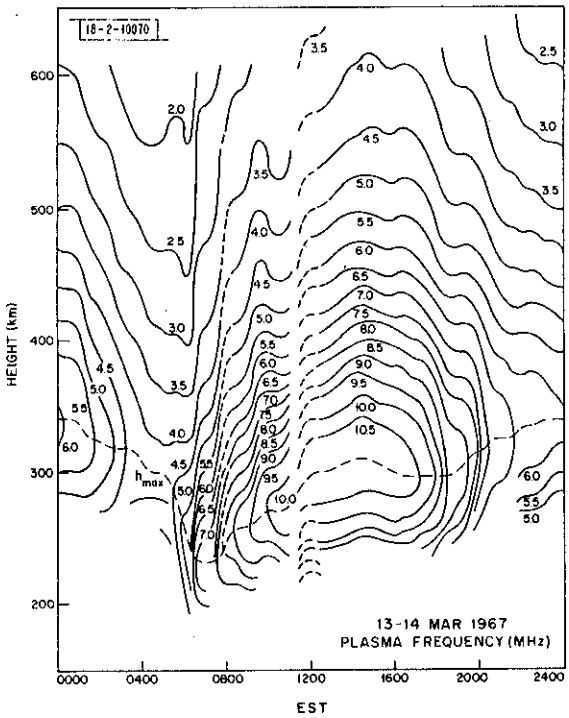

(e)

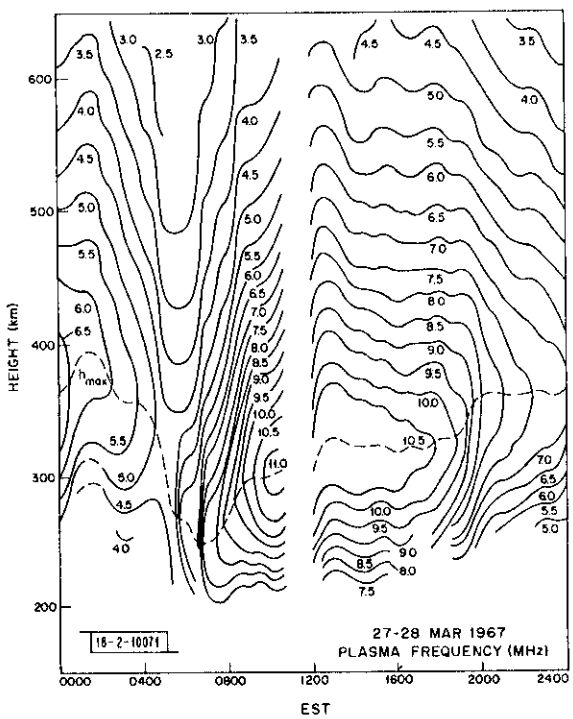

(f)

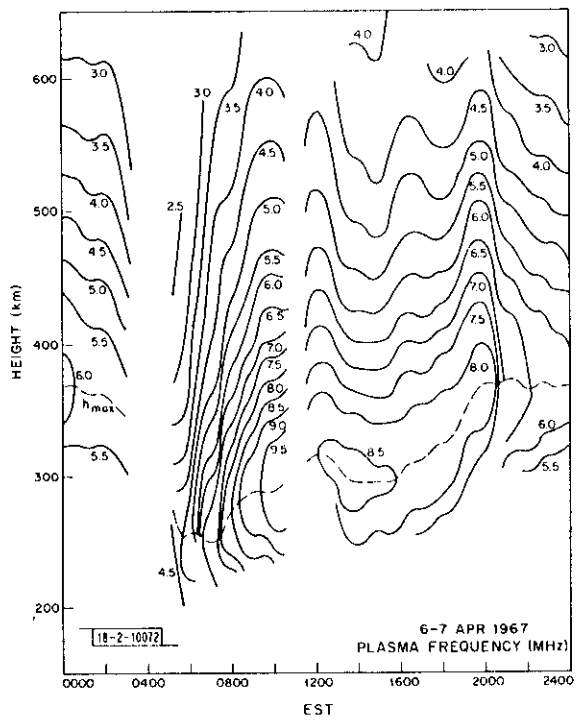

(g)

Fig. 5(a-x). Continued.

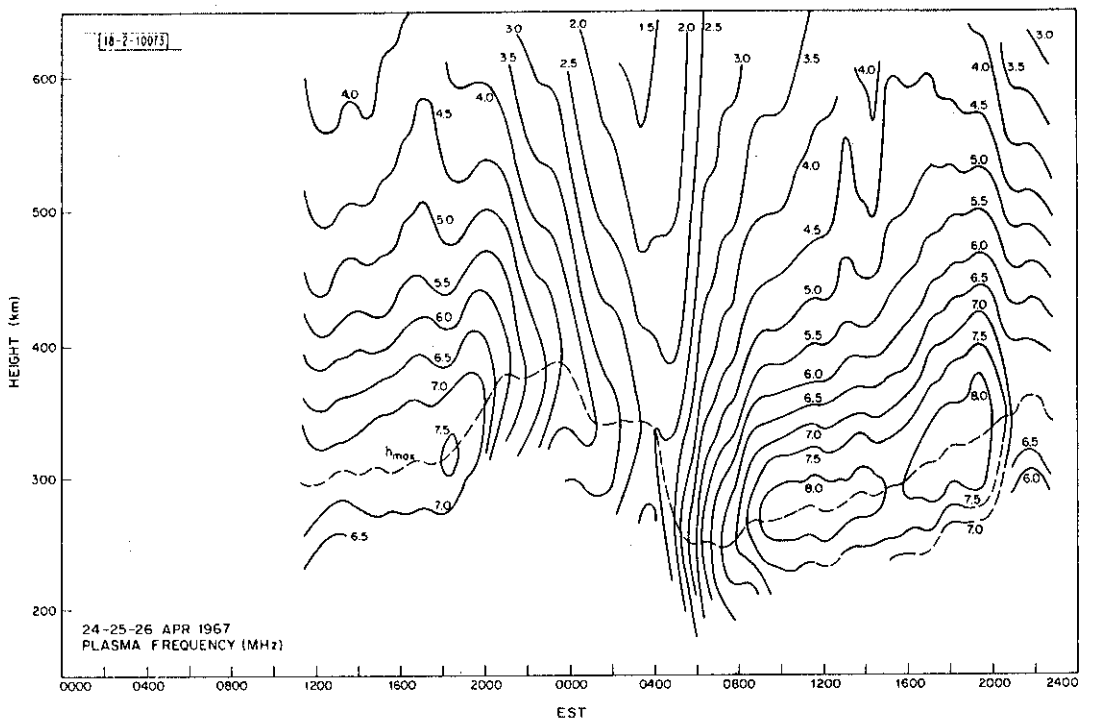

(h)

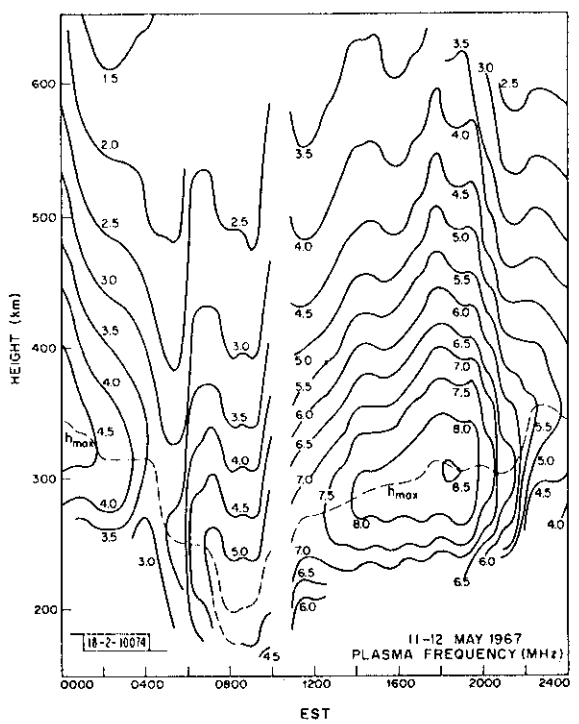

(i)

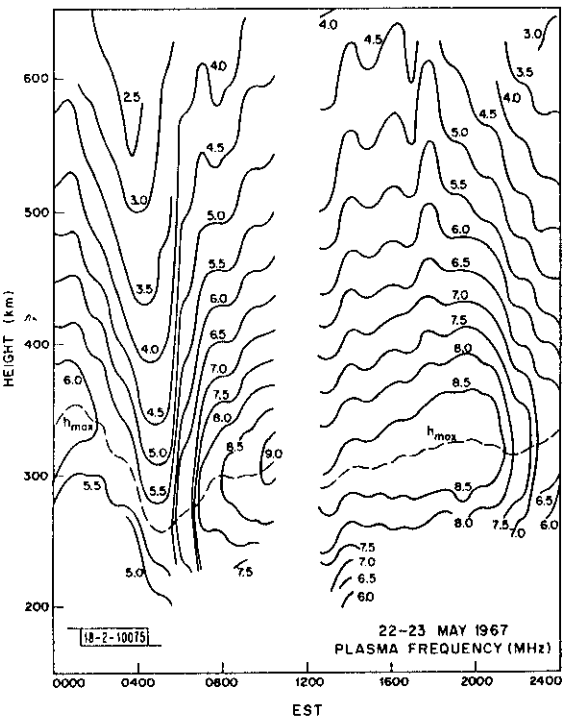

(j)

Fig. 5(a-x). Continued.

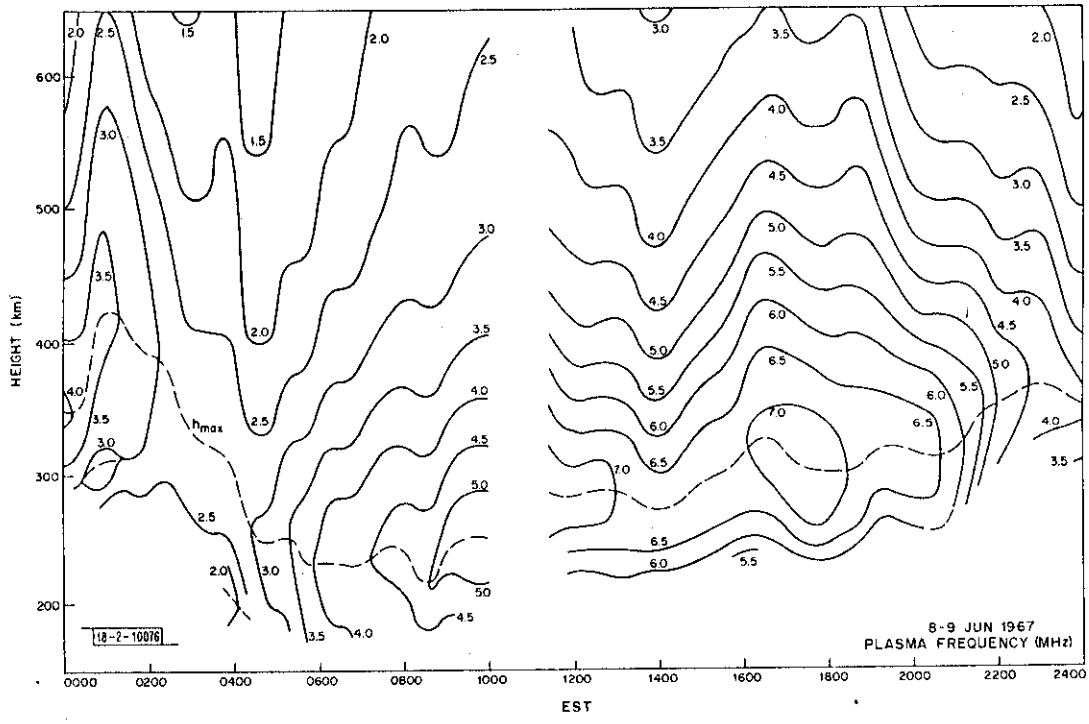

(k)

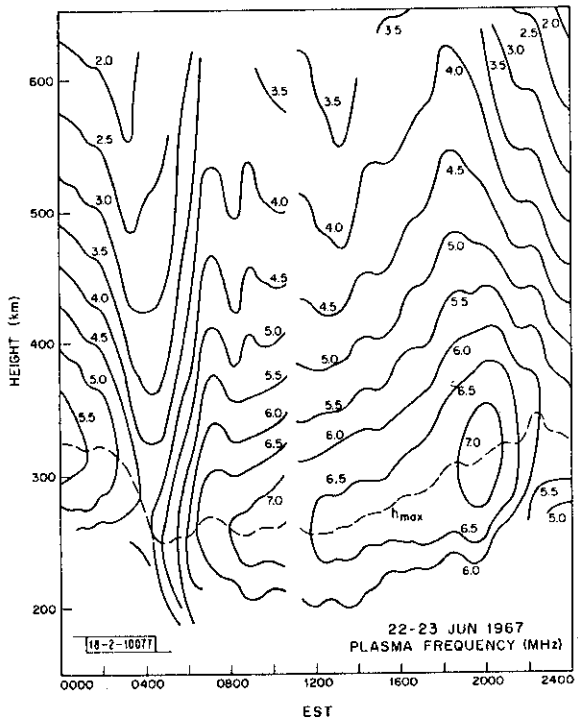

(l)

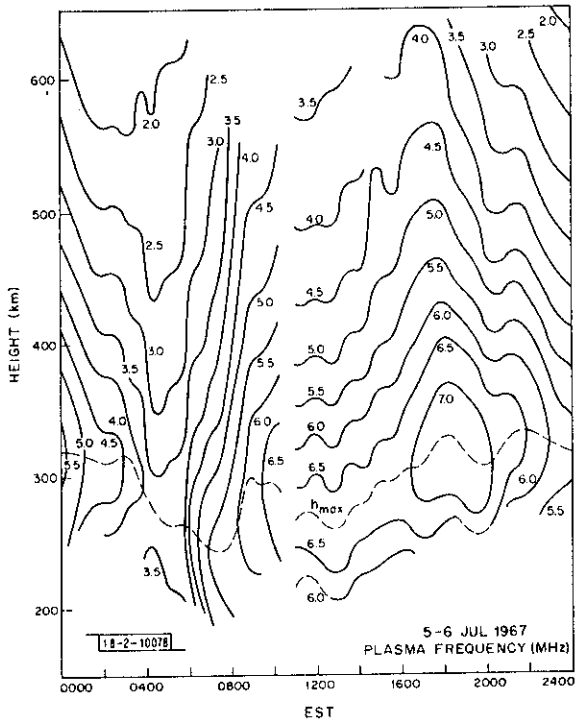

(m)

Fig. 5(a-x). Continued.

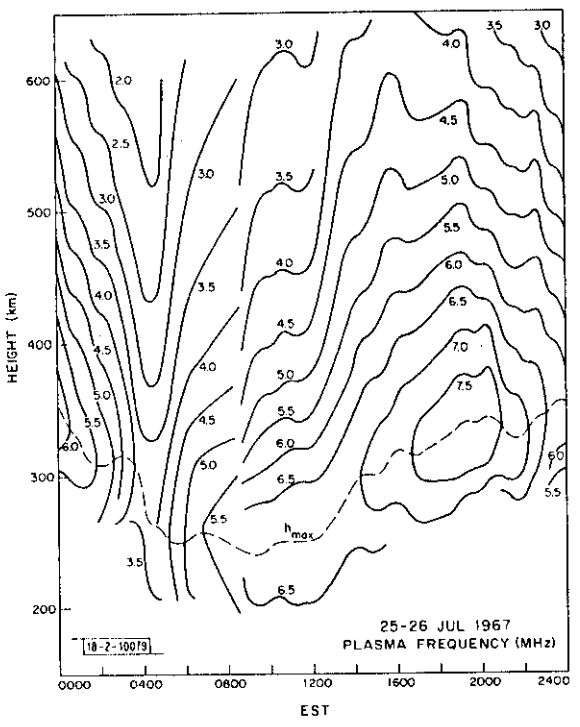

(n)

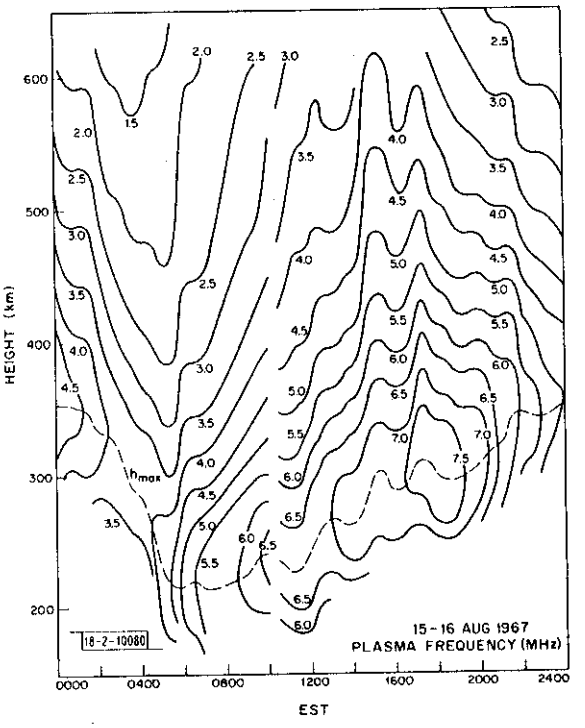

(o)

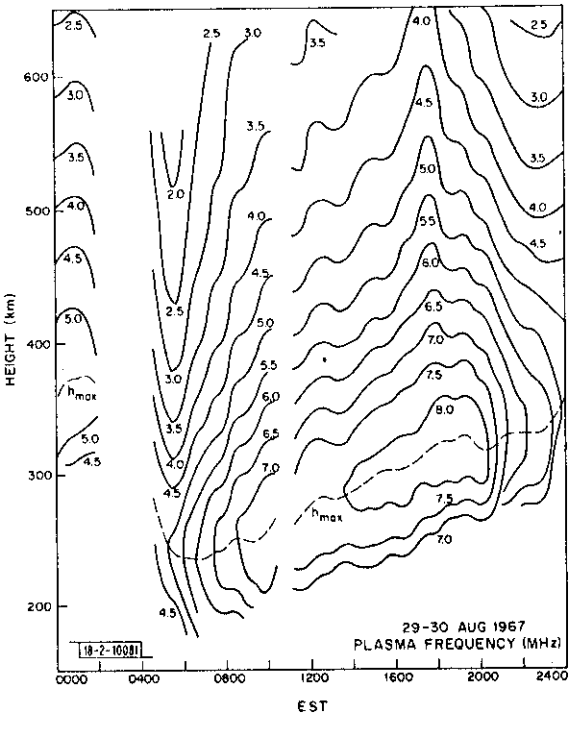

(p)

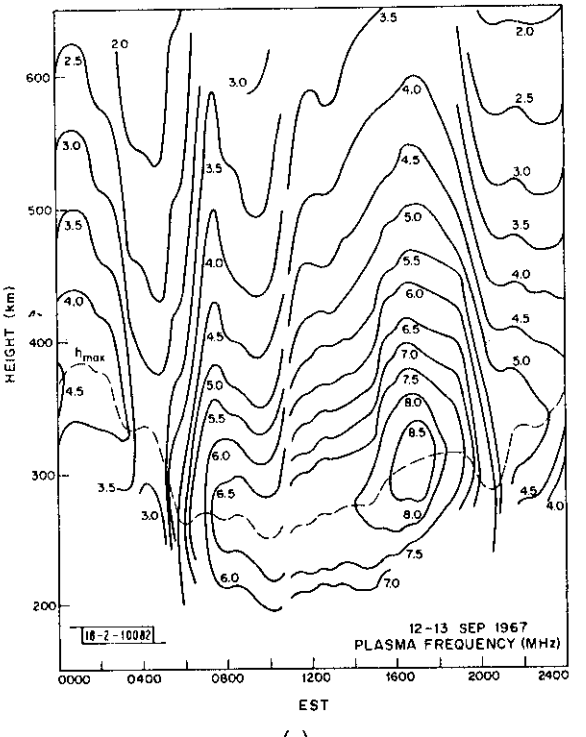

(q)

Fig. 5(a-x). Continued.

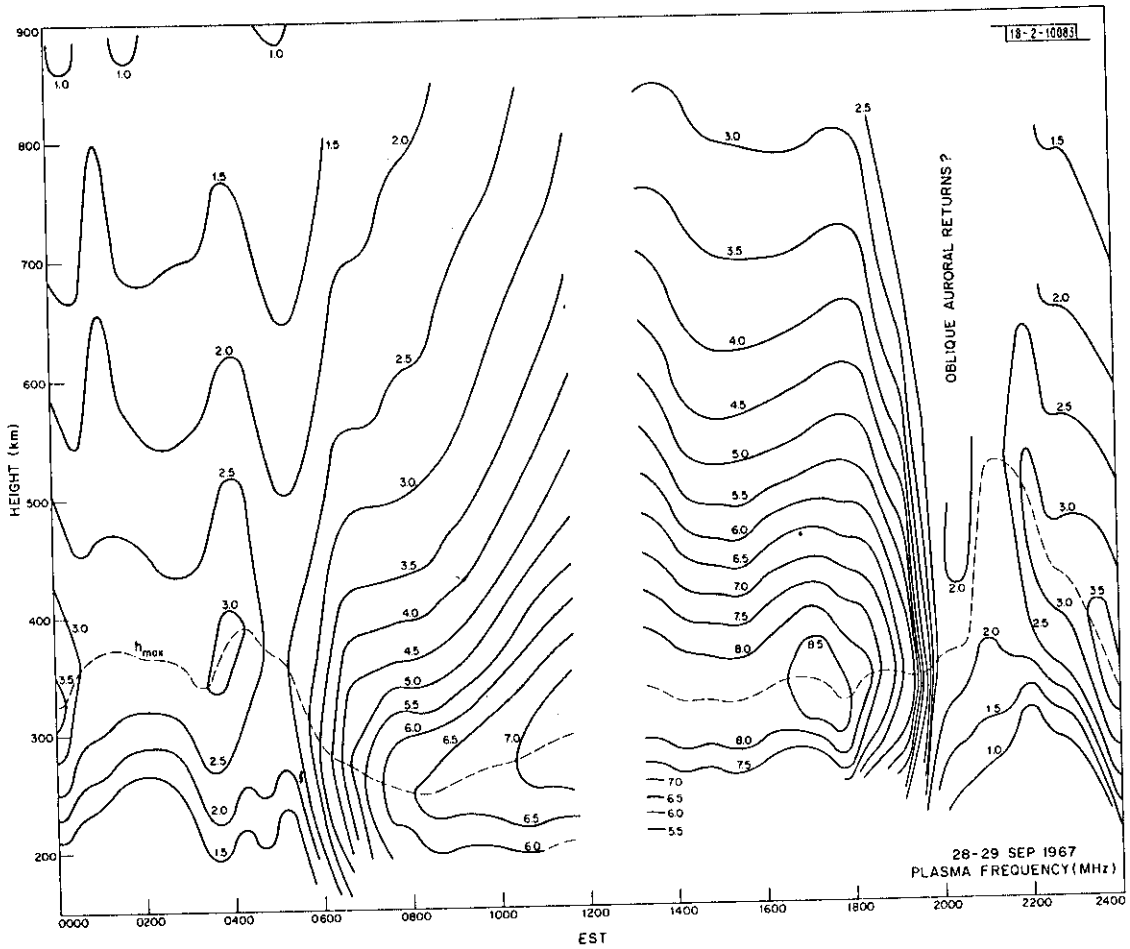

(r)

Fig. 5(a-x). Continued.

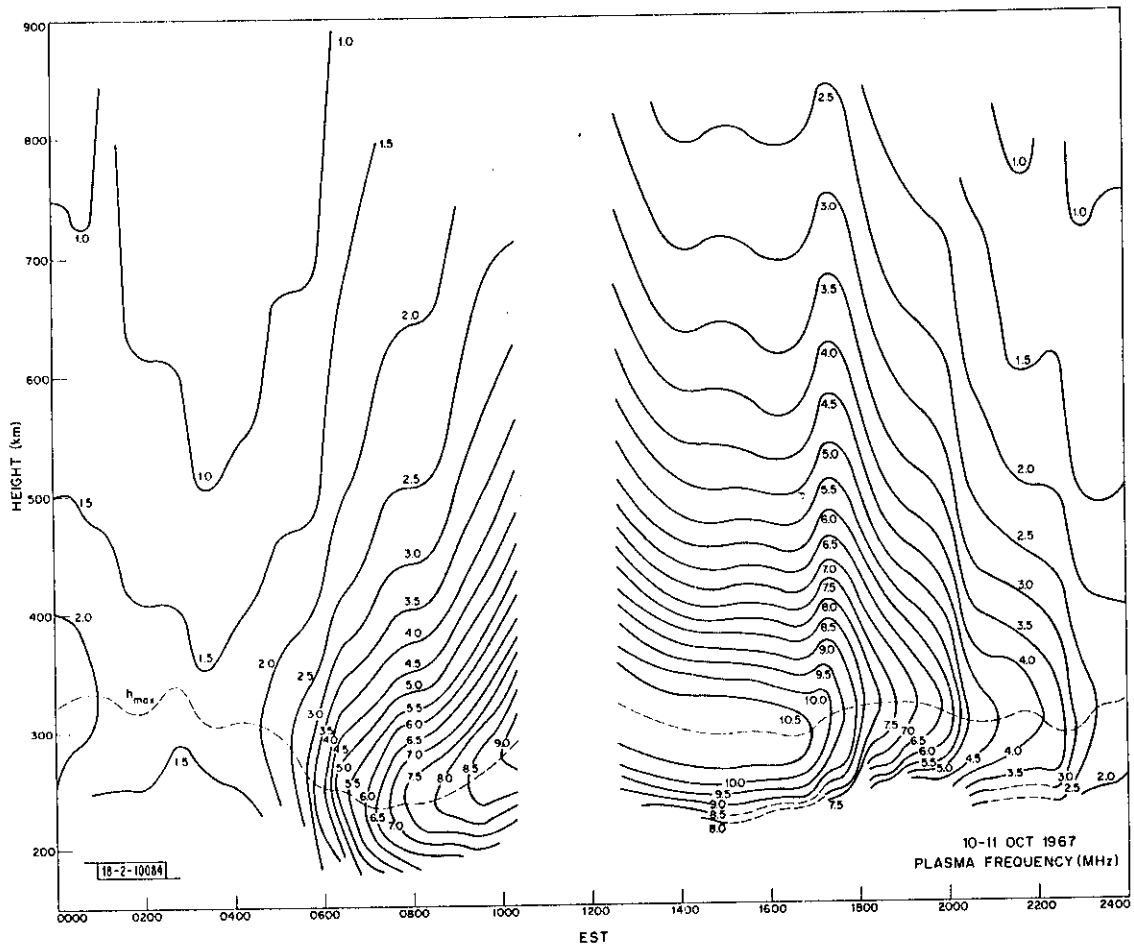

(s)

Fig. 5(a-x). Continued.

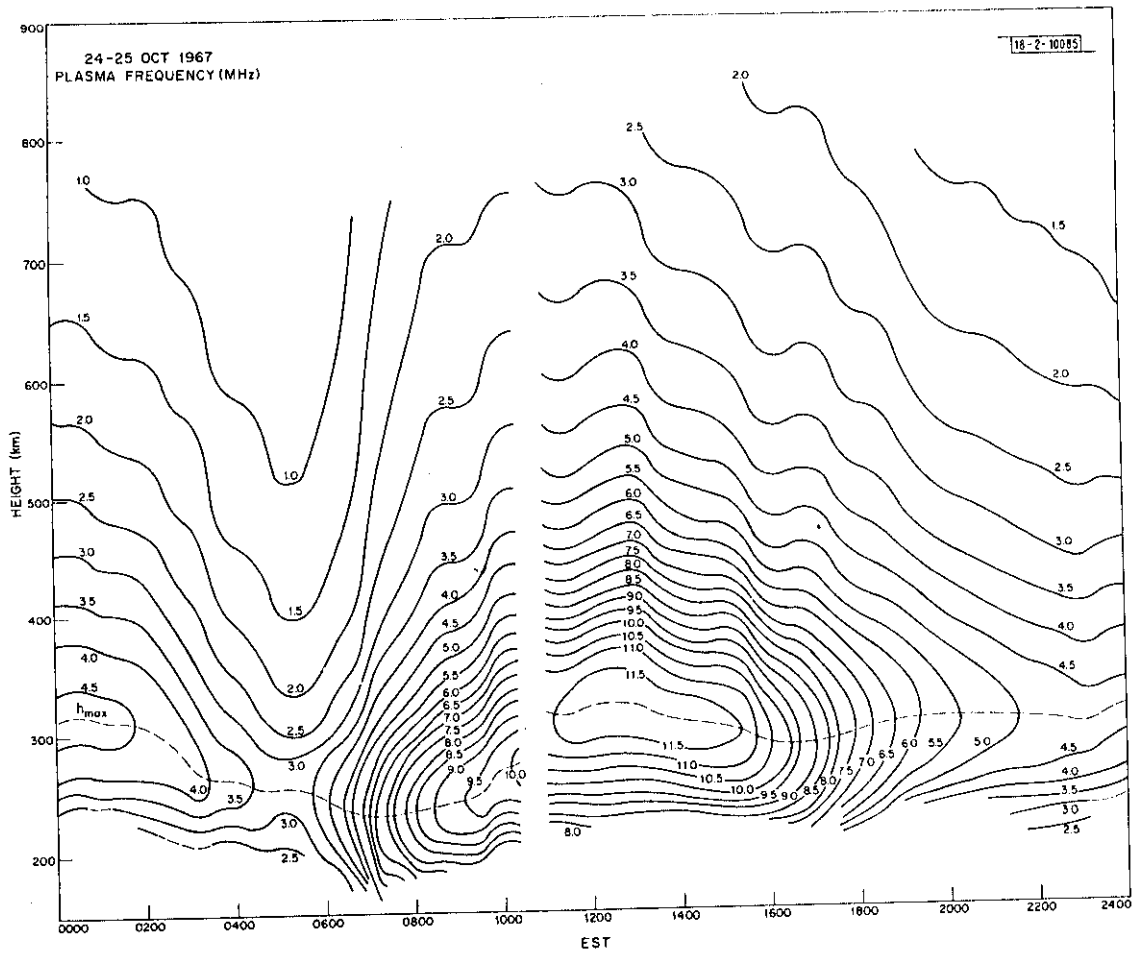

Fig. 5(a-x). Continued.

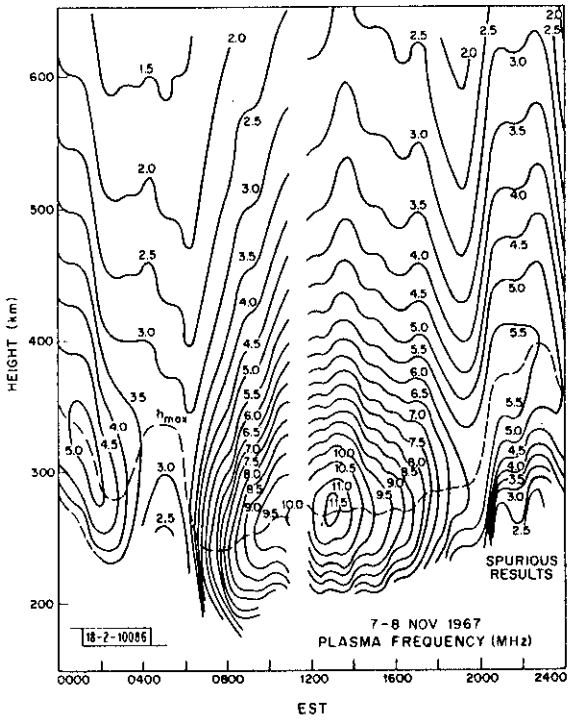

(u)

Fig. 5(a-x). Continued.

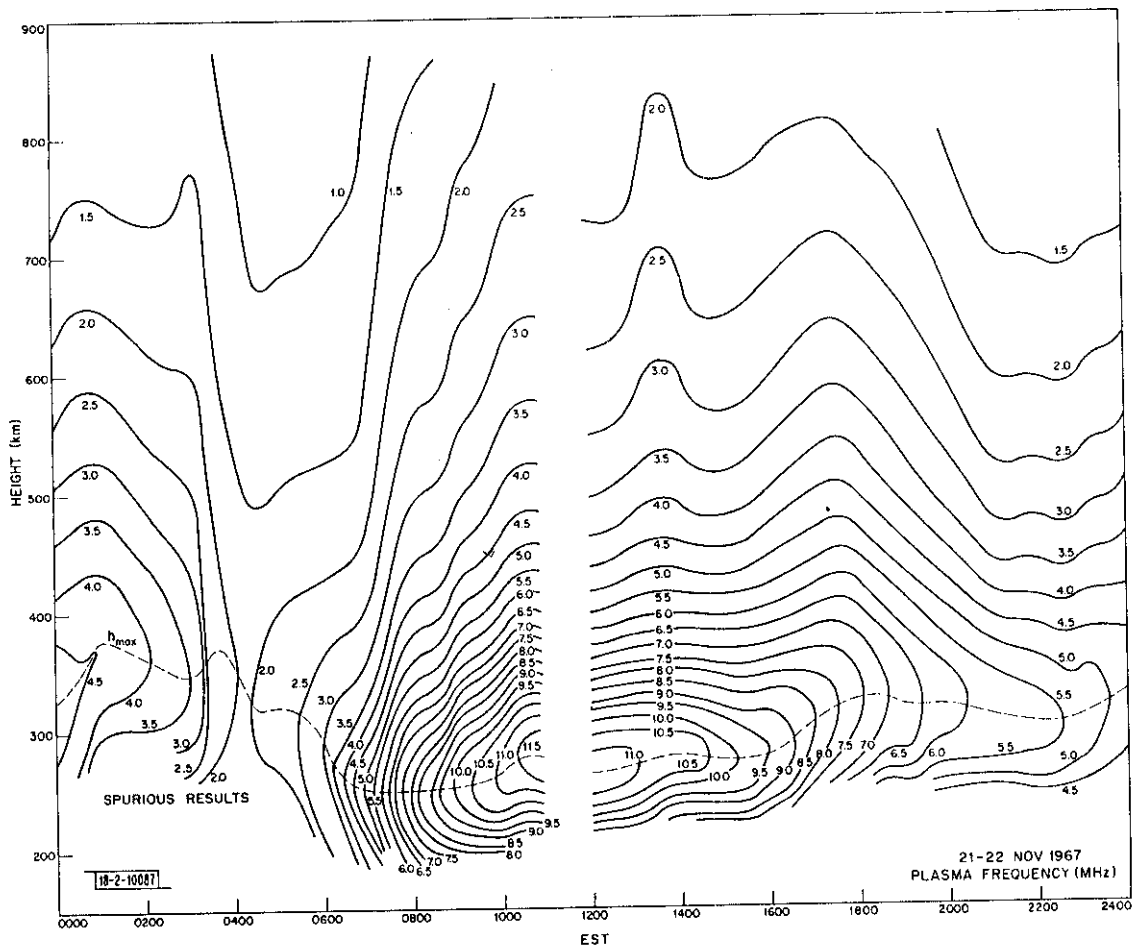

(v)

Fig. 5(a-x). Continued.

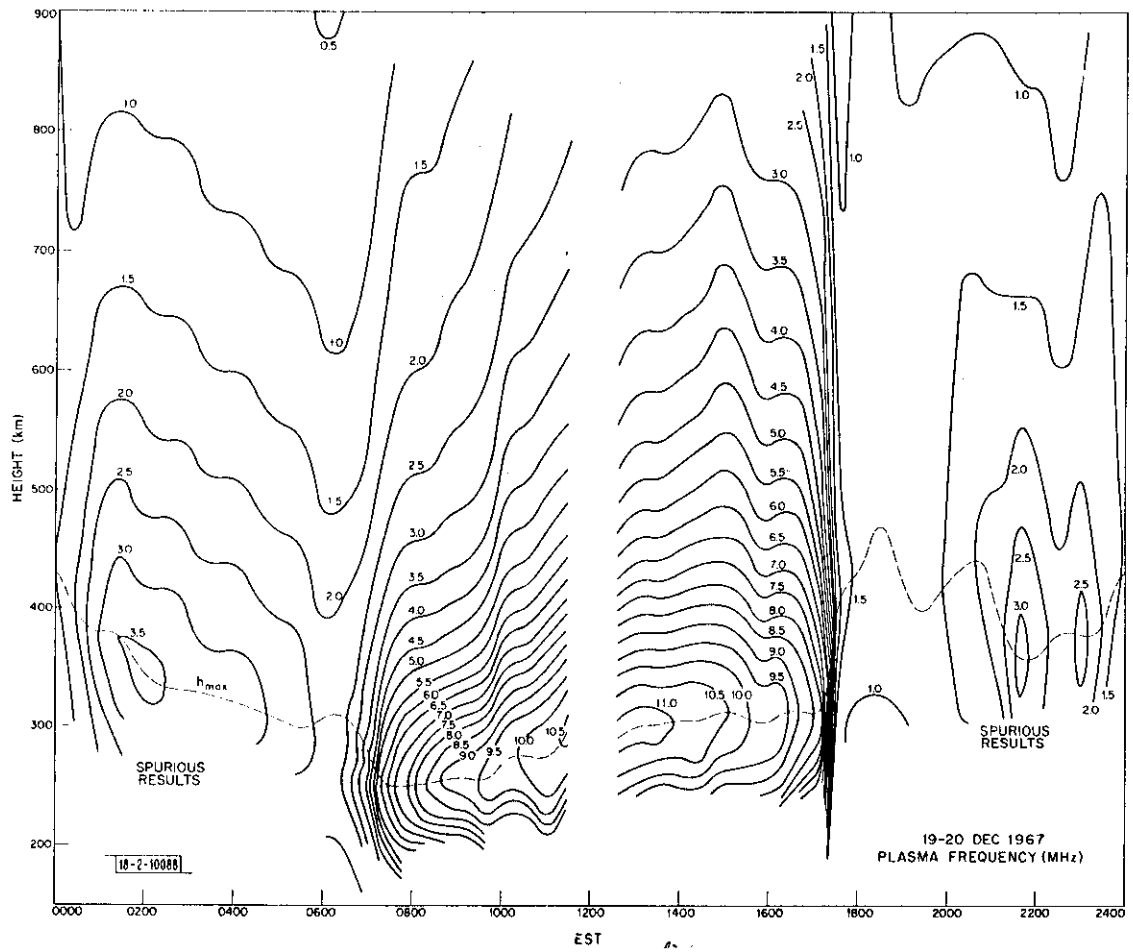

(w)

Fig. 5(a-x). Continued.

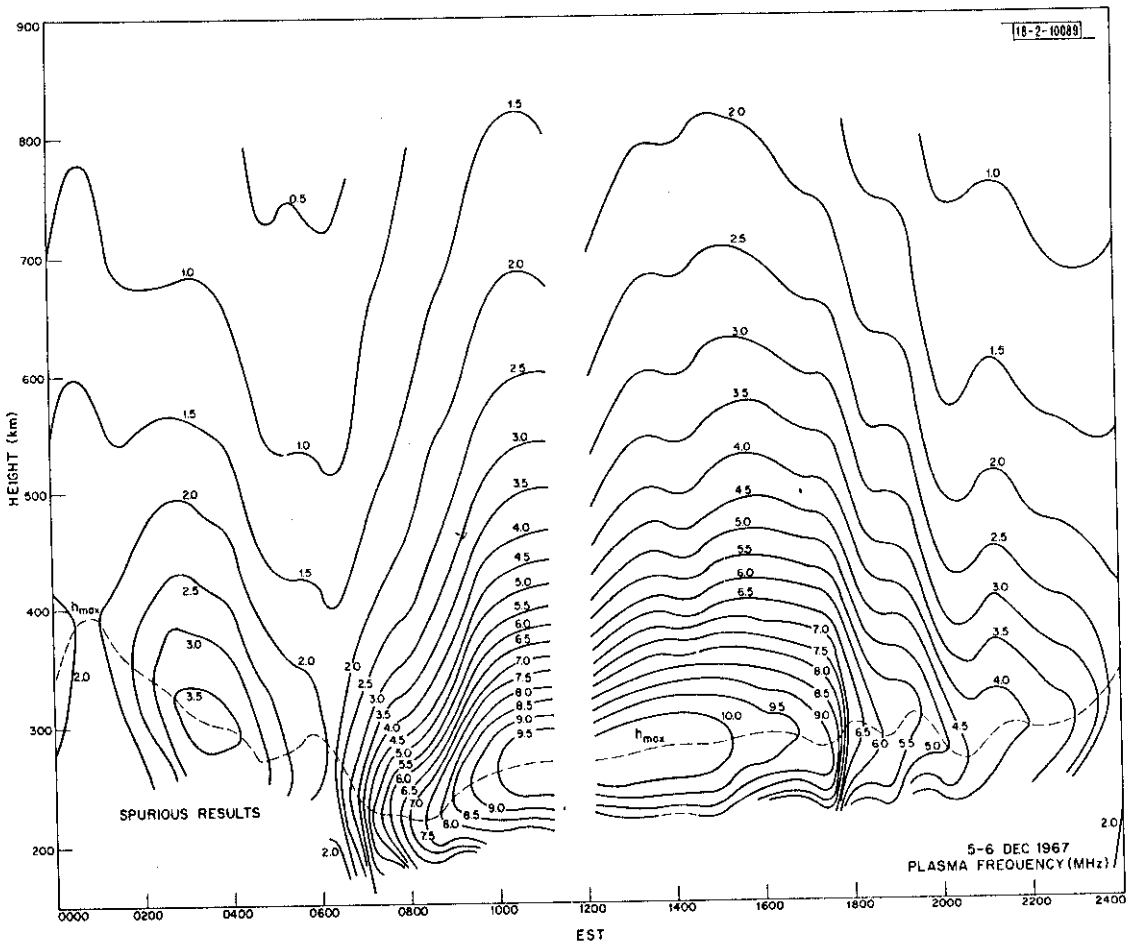

(x)

Fig. 5(a-x). Continued.

TABLE V

SUMMARY OF ELECTRON DENSITY RESULTS AS SHOWN IN FIGS. 5(a) THROUGH (x)

Date (1967)	Noon		Midnight		Comments (hours in EST)	Date (1967)	Noon		Midnight		Comments (hours in EST)
	f_oF2 (MHz)	h_{max} (km)	f_oF2 (MHz)	h_{max} (km)			f_oF2 (MHz)	h_{max} (km)	f_oF2 (MHz)	h_{max} (km)	
5-6 January	10	250	3.5	300	Typical winter behavior: daytime peak f_oF2 at noon; predawn increase at 0200.	5-6 July	6.5	270	5.5	330	Classical summer behavior: marked evening increase.
24-25 January	9.5	230	3.0	300	Typical winter behavior: daytime peak f_oF2 at 1100; predawn increase at 0300.	25-26 July	6.5	250	6.0	350	Summer behavior: marked evening increase.
6-7 February	~10	250	4.5	290	Winter behavior: daytime peak f_oF2 at noon; no predawn increase; slight evening increase above h_{max} F2.	15-16 August	6.5	250	5.0	350	Summer behavior: marked evening increase. Thermal ionic disturbances present?
24-25 February 2 March	~11	300	5.0	330	Winter behavior: daytime peak f_oF2 at 1300.	29-30 August	8.0	280	5.5	350	Summer behavior: marked evening increase.
13-14 March	~11	300	6.0	340	Intermediate behavior: daytime peak f_oF2 at 1430; no evening increase.	12-13 September	8.0	260	4.5	370	Summer behavior: marked evening increase.
27-28 March	~11	325	6.5	360	Intermediate behavior: large values of h_{max} at night. Somewhat disturbed.	28-29 September	8.0	310	3.5	325	Disturbed: rapid fall in f_oF2 at 1900; large fluctuations in h_{max} and N_{max} 2000 to 0100; predawn increase at 0400.
6-7 April	8.5	310	6.0	365	Summer behavior: slight evening maximum. Somewhat disturbed.	10-11 October	10.5	310	2.0	320	Intermediate behavior: very low values of f_oF2 at night.
24-26 April	8.0	275	5.5	380	Summer behavior: evening increase. Somewhat disturbed.	24-25 October	11.5	320	4.5	310	Winter behavior: daytime peak in f_oF2 at 1300.
11-12 May	7.5	275	5.0	345	Storm pattern: large evening increase followed by low values next day.	7-8 November	11.0	270	5.0	350	Winter behavior except for period 2000 to 0200 when layer appears to have been higher than normal.
22-23 May	9.0	300	6.5	340	Summer behavior: slight evening increase.	21-22 November	11.5	270	4.5	325	Winter behavior
8-9 June	7.0	280	4.0	350	Storm pattern: evening increase and abnormally low values next day; very large increase in h_{max} near 0100.	5-6 December	10.5	270	2.0	340	Disturbed: predawn increase near 0300.
22-23 June	6.5	255	5.5	330	Classical summer behavior: marked evening increase.	19-20 December	11.0	290	1.5	425	Very disturbed: very rapid fall in f_oF2 at 1730; predawn increase near 0200.

In previous reports, we identified the typical quiet winter diurnal variation as exhibiting a single daytime maximum near 1300 with a predawn increase in N_{max} usually between 0200 and 0400. Figures 5(a) and (c) provide representative examples of this type of behavior. This winter variation exhibits higher daytime values of N_{max} and lower values of h_{max} than in summer.

The corresponding summer type of behavior exhibits an evening maximum in N_{max} close to the time of ground sunset, and is represented here by Figs. 5(l) and (m). We have discussed previously[3,4] current attempts to understand these divergent types of behavior and the reason for the anomalous variation of N_{max} with season.

The contour diagrams shown in Figs. 5(a) through (x) exhibit more variability from day-to-day than has been encountered previously. This can be attributed to the fact that 1967 was close to the peak of the sunspot cycle.

In June 1965 a large magnetic storm occurred giving rise to a pattern of behavior[8,10] that was observed again on four occasions in 1966 (Ref. 4). This type of behavior is illustrated in Figs. 5(i) and (k). Typically, on the first day of the storm, N_{max} and h_{max} are near their normal levels until late afternoon when both rise to values much larger than normal. On the following morning, h_{max} and N_{max} are depressed considerably below their normal levels, but recover usually during the course of the next 48 hours.

In this report, we present yet a fourth characteristic type of behavior that can be recognized in the contour diagrams. These are the instances when f_oF2 fell extremely rapidly in the late afternoon or evening to abnormally low values ($\leqslant$2 MHz) as illustrated in Figs. 5(r), (s), (w) and (x). The most spectacular example of this, as noted above, occurred on 19 December [Fig. 5(x)], and we note from Table II that this was the most disturbed day in our collection for 1967. On three occasions (28 September, 5 and 19 December), the rapid decrease in f_oF2 was followed by erratic fluctuations in both N_{max} and h_{max}. As suggested above, these may all be instances in which the plasmapause boundary was compressed, so that Millstone successively lay equatorwards of the trough, in the trough and beneath regions of "soft" particle precipitation.

Other instances of peculiar nocturnal behavior were observed in which the layer appears to have been driven to abnormal heights. Examples of this are shown in Figs. 5(k) and (u).

In all, the results presented in Figs. 5(a) through (x) exhibit a rich variety of different types of diurnal variation suggesting that competing forces (neutral air winds, electric fields, particle precipitation) associated with disturbed conditions govern the F-region density in a manner that is not well understood at present.

IV. ELECTRON TEMPERATURE RESULTS

A. Electron Temperature Profiles

The lowest altitude at which the electron temperature is measured is 225 km. To extend the results to lower altitudes, a smooth curve has been drawn from the temperature observed at 225 km to an assumed value T_e = 355°K at 120 km where temperature equilibrium is believed to exist. These electron temperature profiles were then employed to construct contour diagrams of T_e vs height and time. These are presented in the next section.

B. Electron Temperature Contour Diagrams

Figures 6(a) through (w) present the contour diagrams for T_e and Table VI summarizes the main features of these results. Owing to the large winter daytime values of N_{max}, the electron

TABLE VI

SUMMARY OF ELECTRON TEMPERATURE RESULTS
AS SHOWN IN FIGS. 6(a) THROUGH (w)

Date (1967)	Comments (hours in EST)
5-6 January	Daytime results missing; morning maximum near 0800.
24-25 January	Data missing.
6-7 February	Morning maximum near 0800; afternoon values low.
24-25 February 2 March	Morning maximum near 0700; temperature inversion near 275 km at 1100.
13-14 March	Morning maximum near 0700; temperature inversion near 275 km at 1100 to 1400.
27-28 March	Morning maximum near 0600; temperature inversion near 300 km at 1000 to 1300; slight nocturnal increase beginning at 2100.
6-7 April	Morning maximum near 0600; no temperature inversion.
24-26 April	Slight morning maximum near 0700.
11-12 May	Classical storm behavior: afternoon values abnormally low; very much larger than normal values next morning.
22-23 May	Morning maximum near 0530.
8-9 June	Clear case of nocturnal heating 0000 to 0300.
22-23 June	Quiet summer day variation: high daytime values.
5-6 July	Quiet summer day variation: high daytime values.
25-26 July	Very high daytime temperatures.
15-16 August	Low afternoon temperatures associated with large evening increase; somewhat similar to 11-12 May.
29-30 August	Normal summer behavior.
12-13 September	Normal summer behavior though minor increase near midnight.
28-29 September	Very erratic behavior between 1600 and 0600: marked increase beginning near 2000 and reaching a peak at 2045; less marked increase beginning at 0300.
10-11 October	Very abnormal behavior after 1800: marked increases beginning near 2000 and 2200; nighttime values far exceed daytime values.
24-25 October	Temperature inversion 1100 to 1500 centered at 350 km.
7-8 November	Temperature inversion 1000 to 1300 centered at 275 km; morning maximum near 0700.
22-23 November	No temperature inversion; pronounced nocturnal increase beginning near 0300.
5-6 December	No temperature inversion; nocturnal increase 2300 to 0200; morning maximum near 0700.
19-20 December	Very disturbed: marked temperature surge 1800 to 2000; weaker one 2200 to 0100.

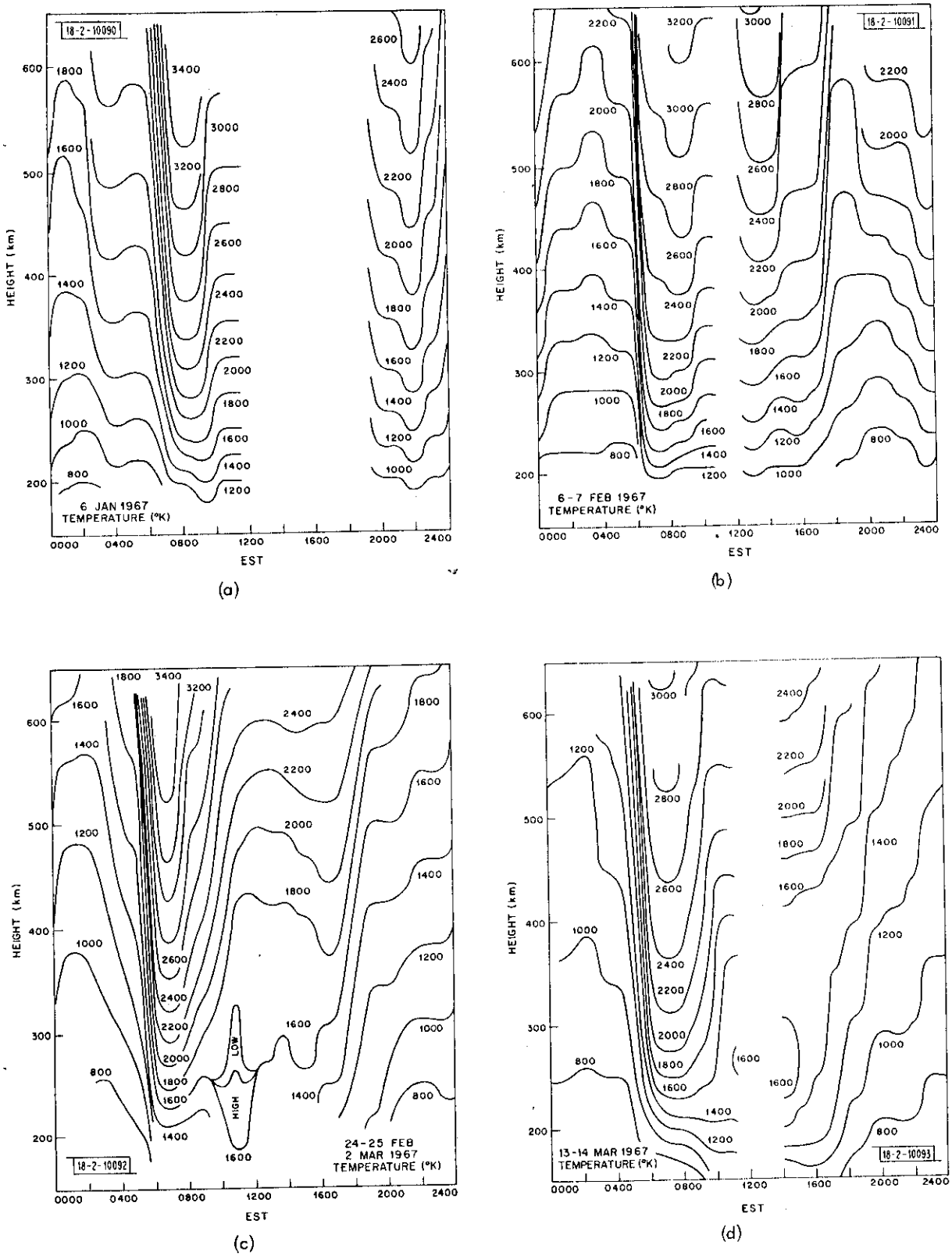

Fig. 6(a-w). Contour diagrams of constant electron temperature as a function of height and time for each of the observing periods.

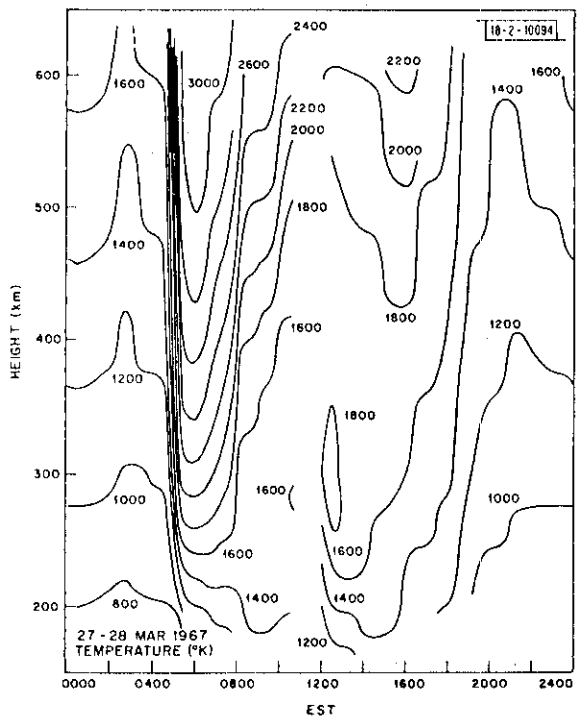

(e)

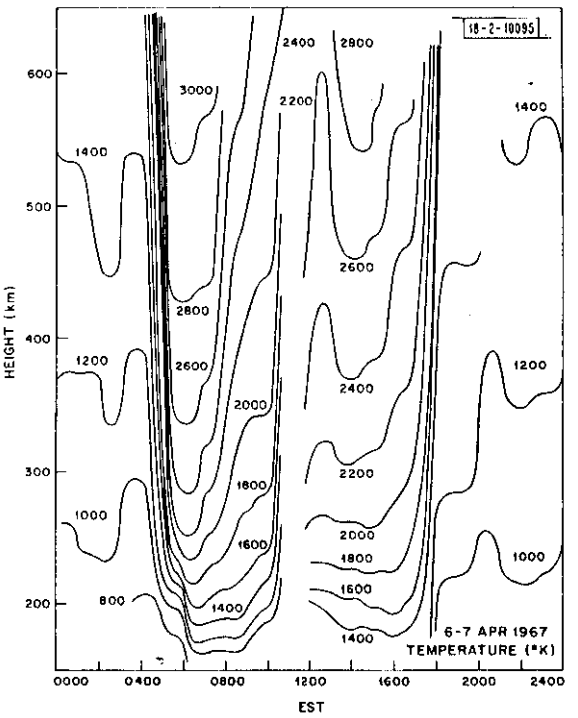

(f)

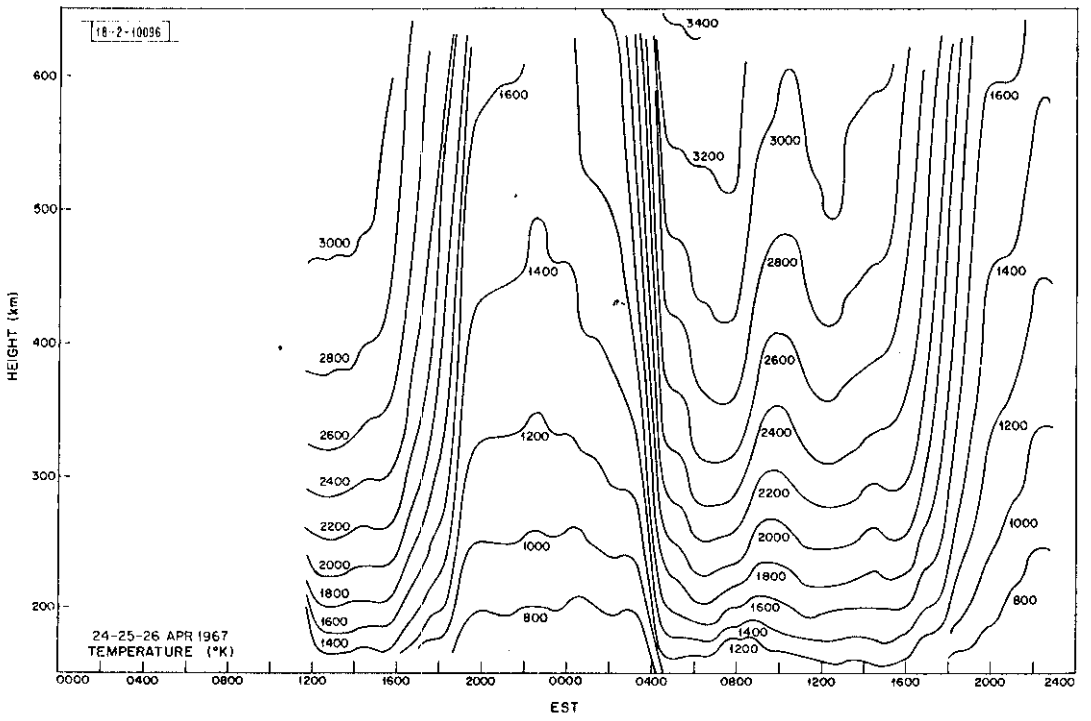

(g)

Fig. 6(a-w). Continued.

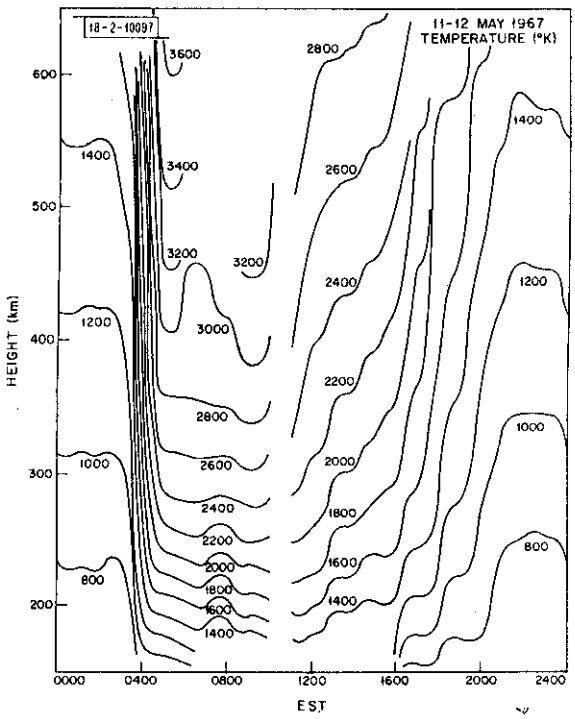

(h)

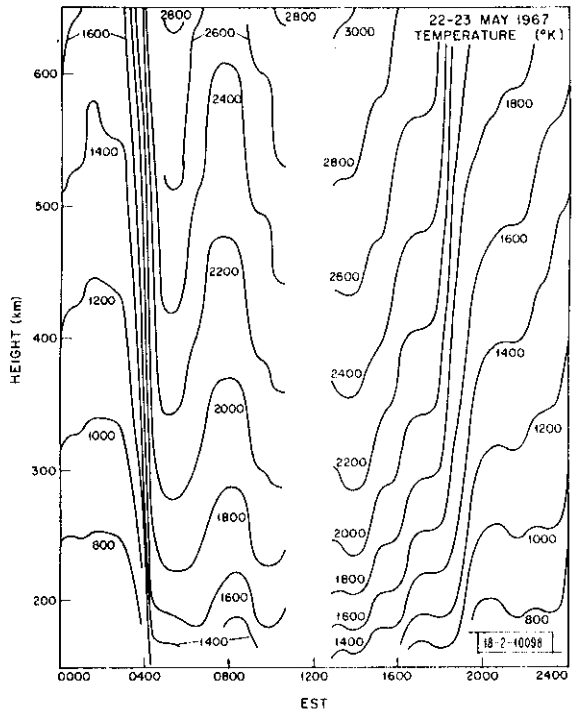

(i)

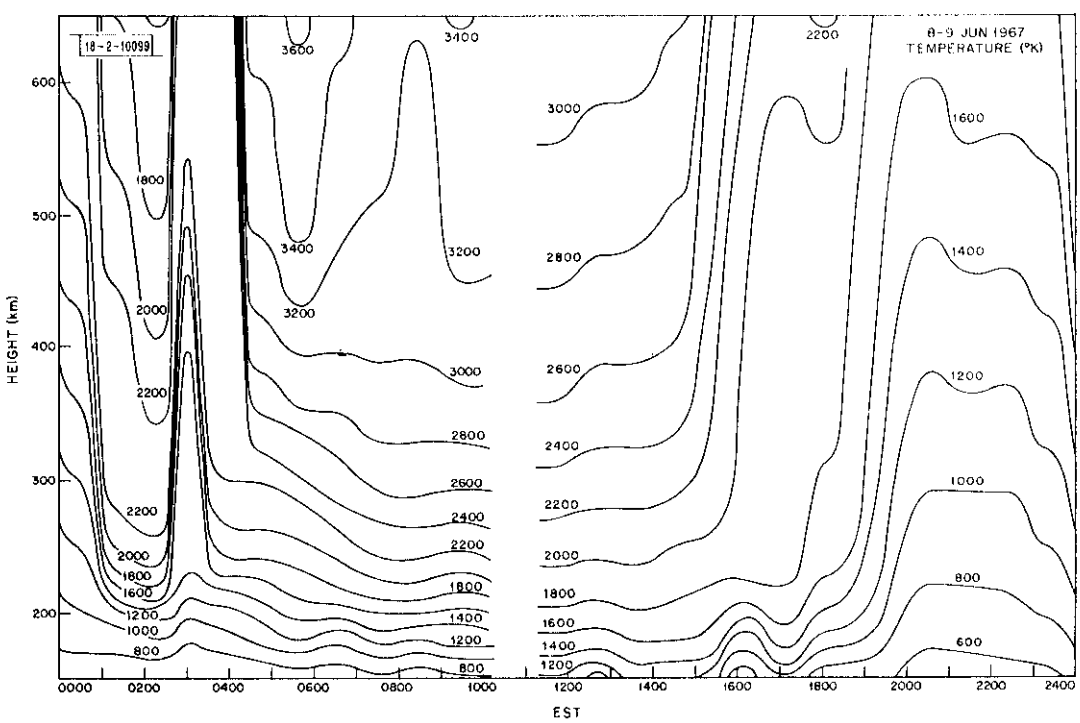

(j)

Fig. 6(a-w). Continued.

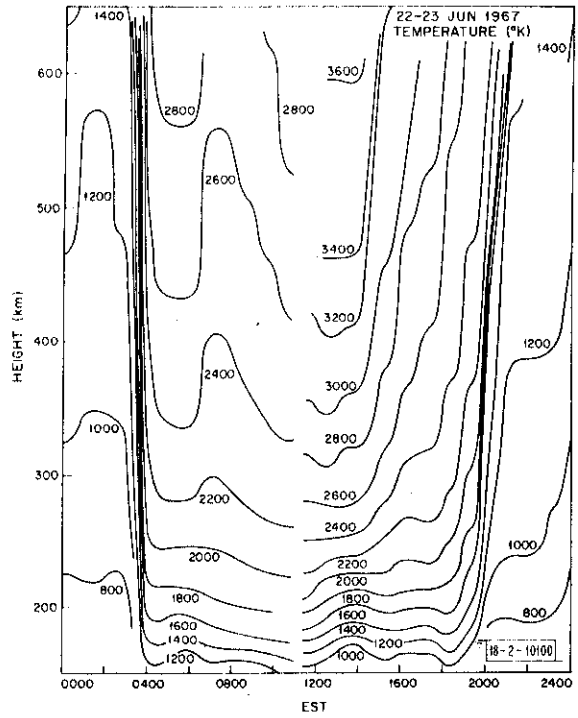

(k)

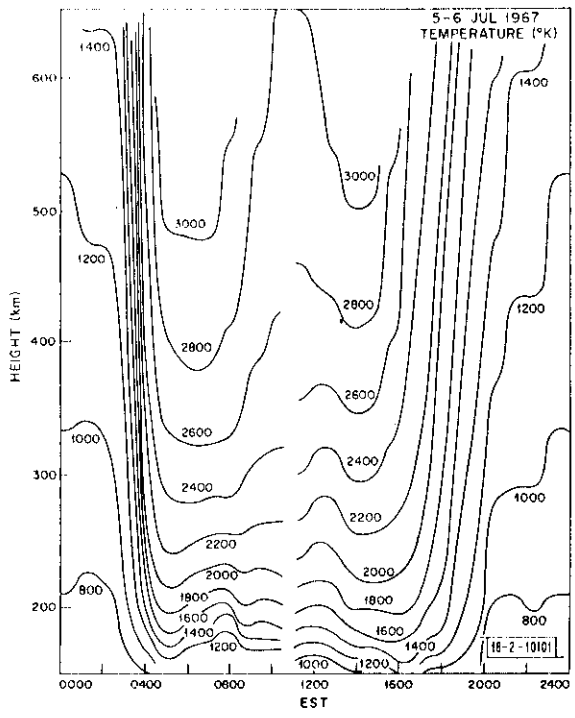

(l)

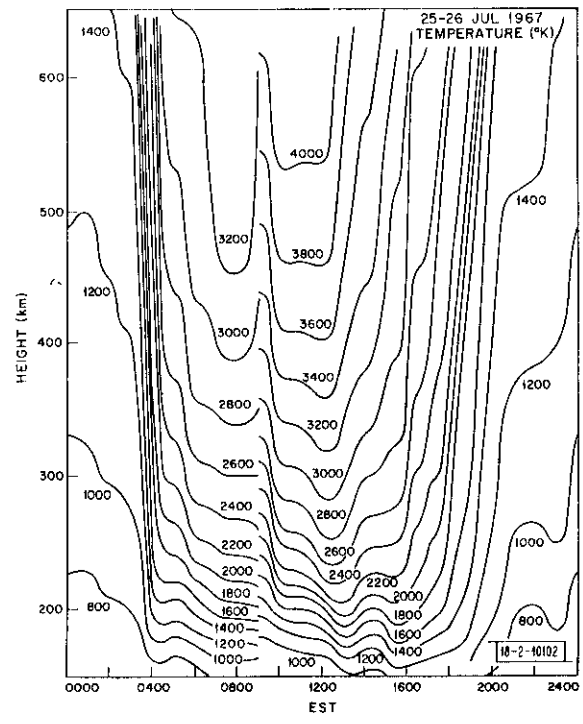

(m)

Fig. 6(a-w). Continued.

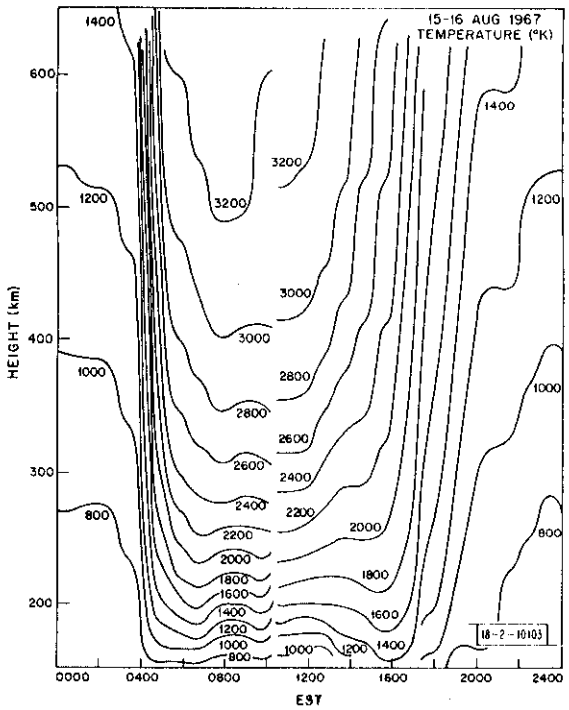

(n)

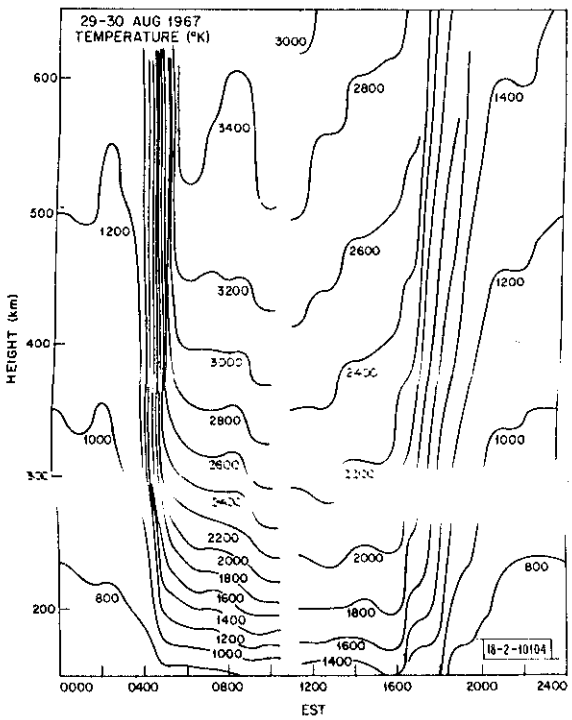

(o)

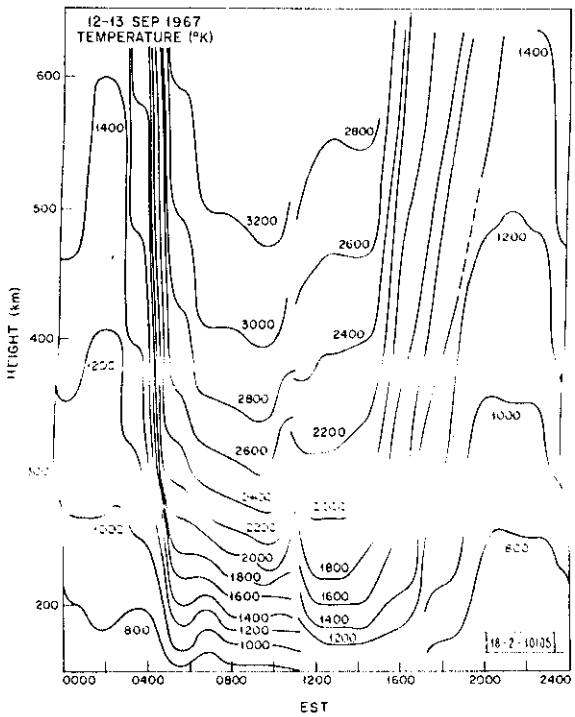

(p)

Fig. 6(a-w). Continued.

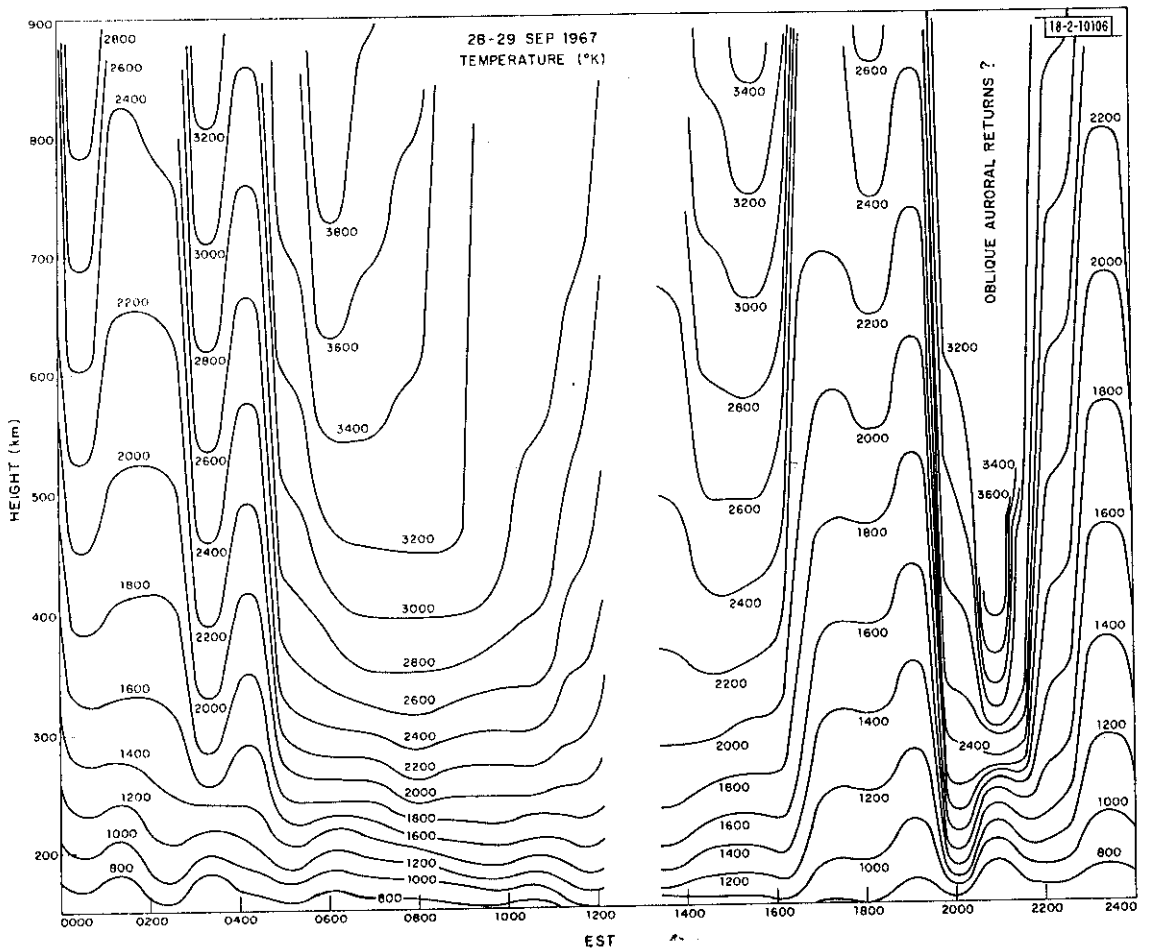

(q)

Fig. 6(a-w). Continued.

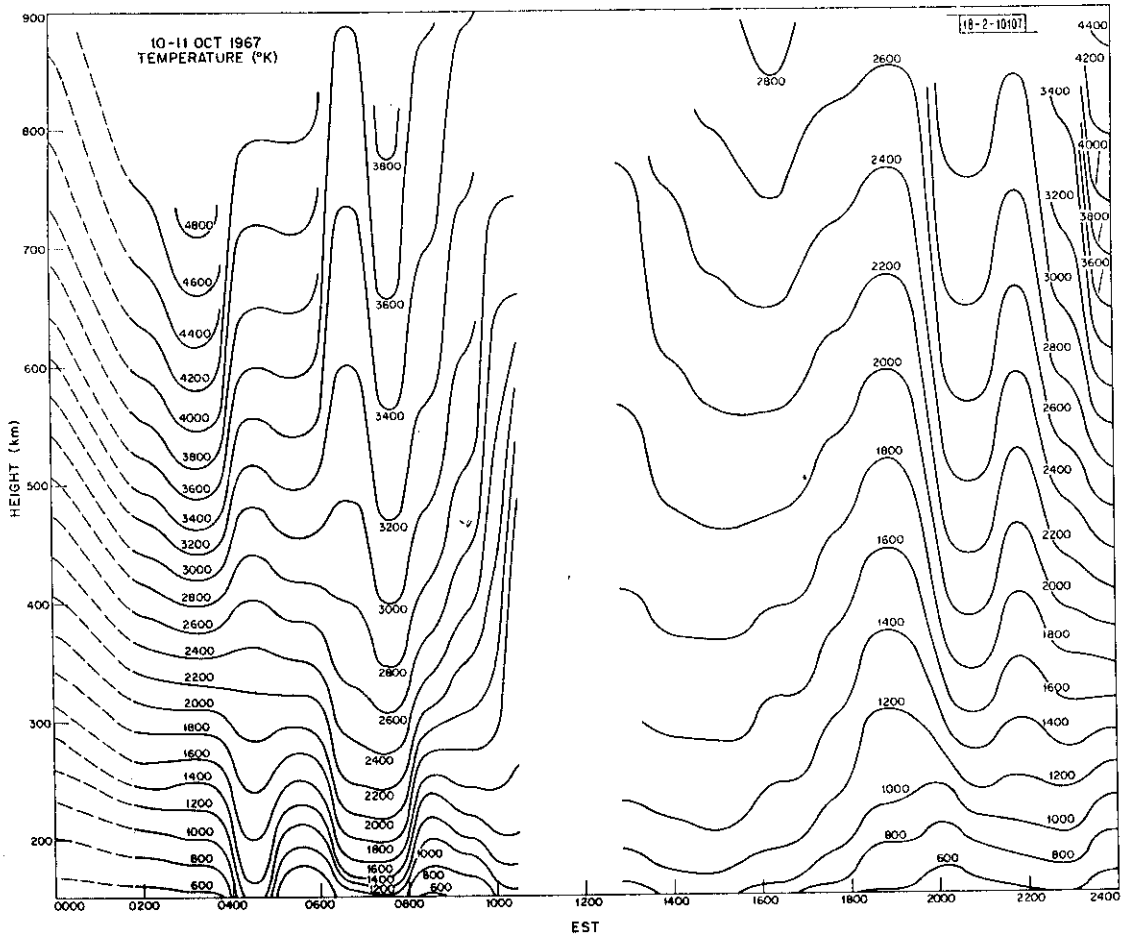

(r)

Fig. 6(a-w). Continued.

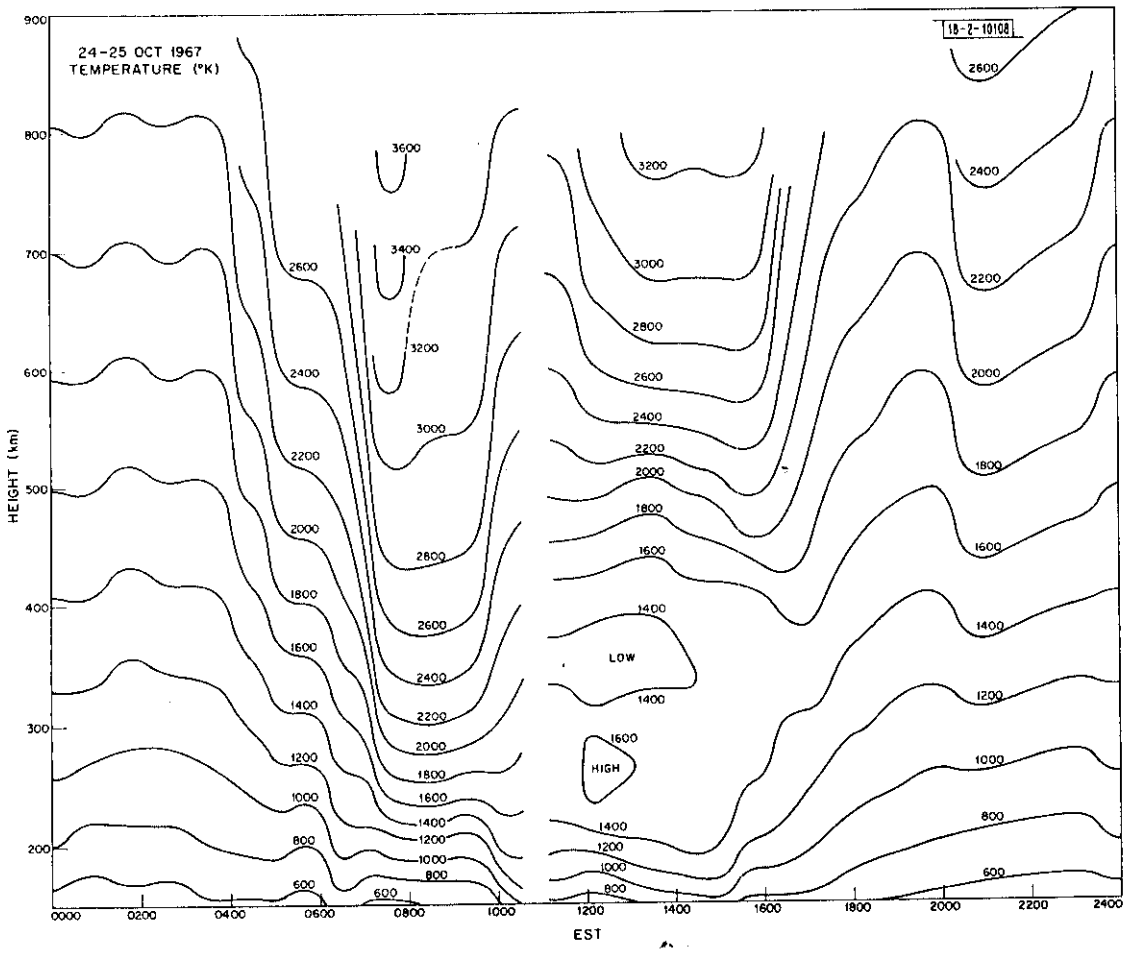

Fig. 6(a-w). Continued.

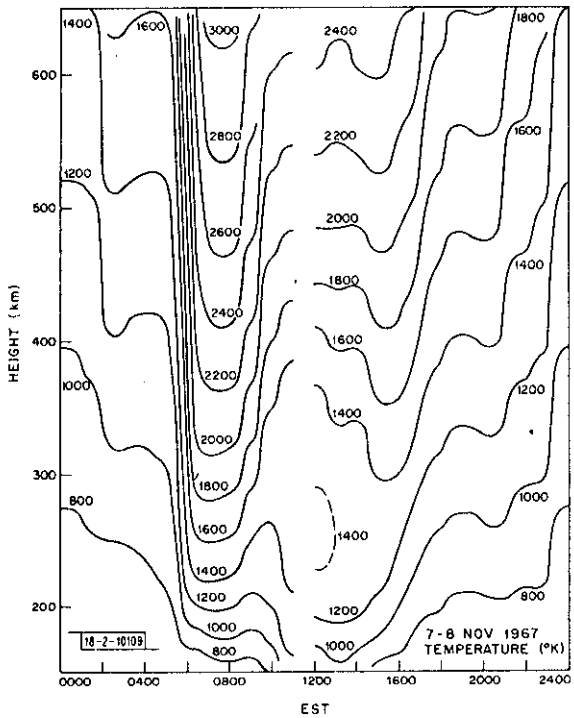

(t)

Fig. 6(a-w). Continued.

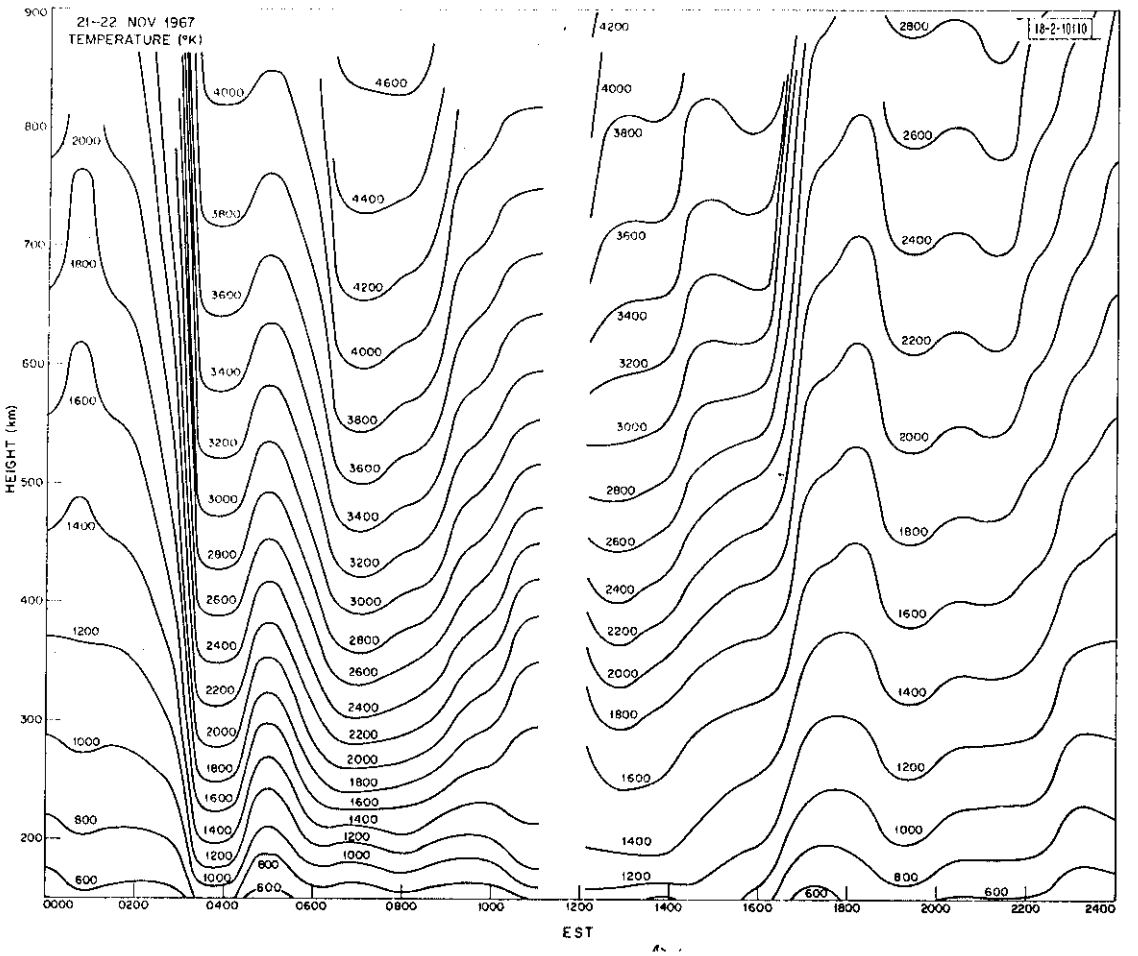

(u)

Fig. 6(a-w). Continued.

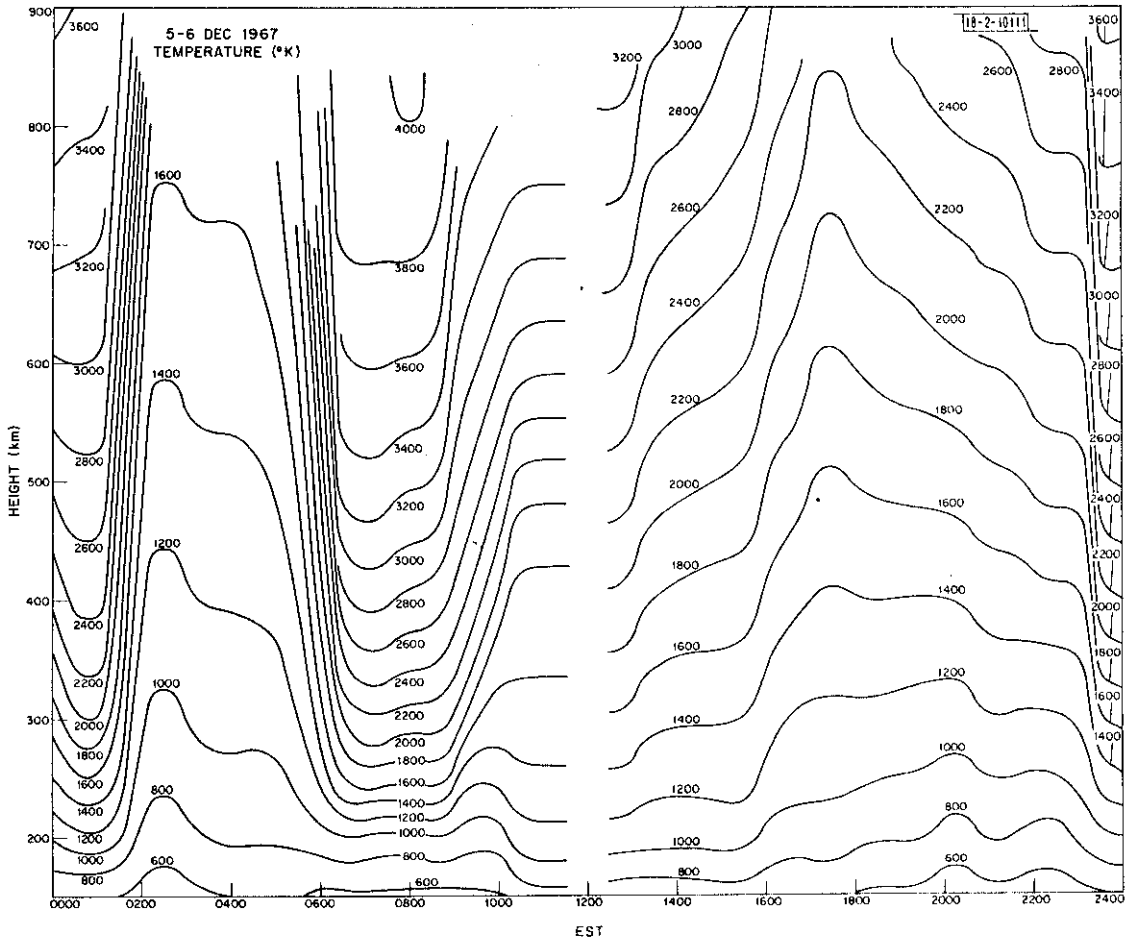

(v)

Fig. 6(a-w). Continued.

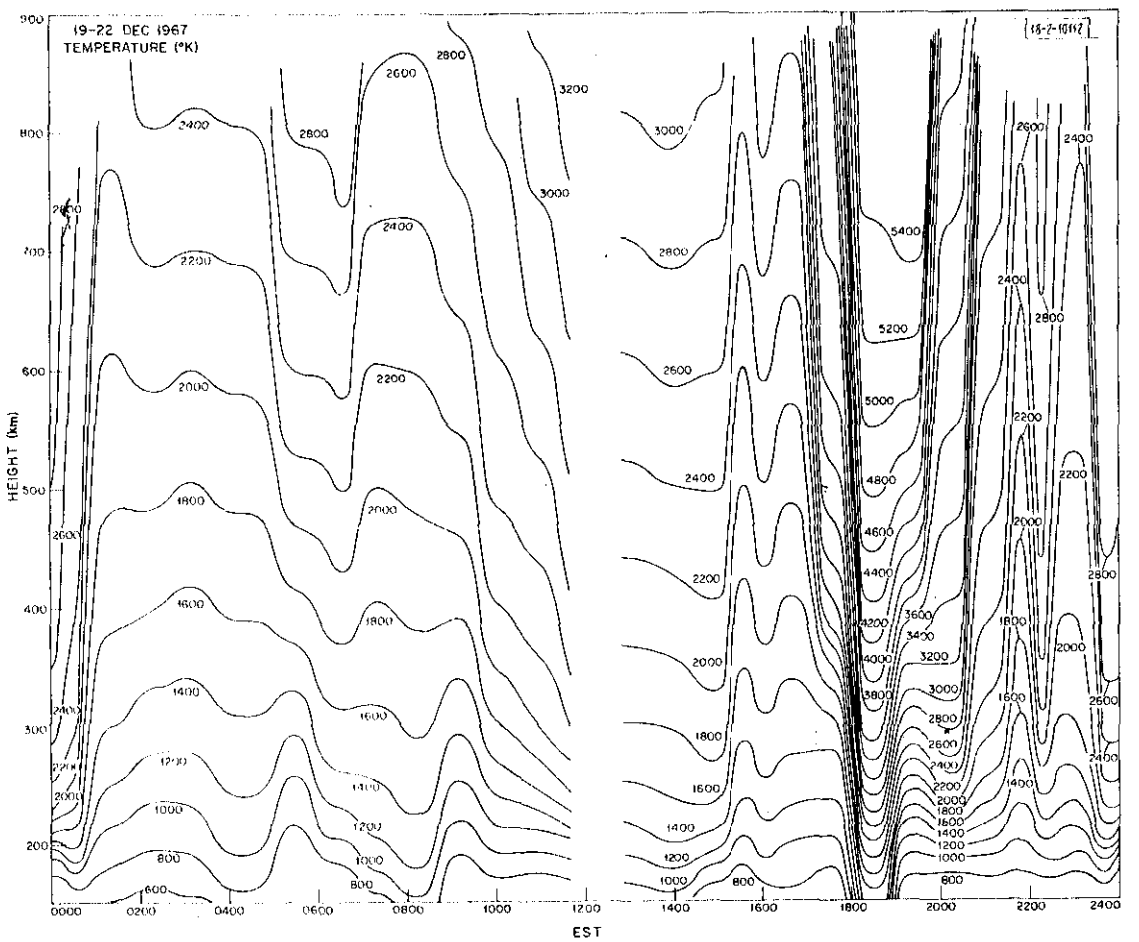

(w)

Fig. 6(a-w). Continued.

temperature near 300 km was frequently lower at midday than shortly after sunrise. That is, the electron temperature is often found to exhibit a morning maximum as illustrated in Fig. 6(b). This morning maximum is especially pronounced on those days [e.g., Fig. 6(c), (d), (s)] when there was an inversion in T_e near 300 km that appears when the local electron density $\geq 10^6$ el/cm^3. This inversion is brought about by heat lost to the ions via coulomb encounters. However, owing to the limited height resolution of the measurements ($\geq$75 km) we do not believe that the full extent of this minimum was ever explored. We first encountered this type of behavior at Millstone in December 1966.[4]

Anomalous behavior of the electron density has caused anomalous temperature variations. As a rule, high electron temperatures accompanied lower than normal electron densities and vice versa. Figure 6(h) provides a good example of this pattern. On this day, the electron density rose to unusually large values in the afternoon causing a decrease in T_e long before sunset. The next morning the density was abnormally low and the temperature much higher than normal.

Instances of nocturnal heating associated with geomagnetically disturbed conditions appear to have been common. The clearest example of this is 8-9 June [Fig. 6(j)], where shortly before midnight T_e began to increase and by 0200 had reached essentially the same values as during the daytime. Other instances occurred later in the year, e.g., 28-29 September, but are not always easily recognized because the winter nighttime values of T_e are high at Millstone. During winter the sun remains above the horizon at the conjugate point causing heating of the protonosphere via fast photoelectrons and heating of the local ionosphere through conduction from the protonosphere.

Virtually all nocturnal increases in temperature are associated with extremely low values of density. In some cases this may be because the trough region moved over Millstone and, as shown by satellite results,[17] the electron temperature is consistently higher on the poleward side of the trough region or plasmapause. On other occasions nocturnal temperature increases may have been caused by heat deposited in the magnetosphere by injection of energetic particles into the ring current.[9] These particles are then damped through ion cyclotron waves and feed energy into the ambient plasma which is conducted down field lines into the magnetosphere. This theory, developed by Cole[18] to explain the stable red arc, would suggest that ring current particles within the plasmapause decay more rapidly than outside, and thus the heat injection must be greatest near the boundary.

C. Average Temperature Profiles

In previous years, it was noted that during the day and for much of the night T_e and T_i were relatively constant, and hence we constructed average temperature profiles for the periods 1000 to 1500 (day) and 2100 to 0300 (night) which served to show seasonal variations. We have continued this practice for the data collected in 1967, although the rationale for so doing is weakened by the variation of T_e on winter days (when $f_0F2 > 10$ MHz and a temperature minimum appears) and by cases of nocturnal heating; both effects cause appreciable changes in T_e within the averaging interval.

To construct these average temperature profiles, values of T_e were read off the temperature profiles obtained each half hour during the above periods at 100-km intervals. These were then averaged, plotted and smooth curves drawn through the points. Figures 7(a) through (z) show the results. In general, these curves present no major surprises, though for the first time we encountered a case where the average daytime temperatures at some altitudes were less than the nighttime temperatures. This occurred on 10-11 October [Fig. 7(u)].

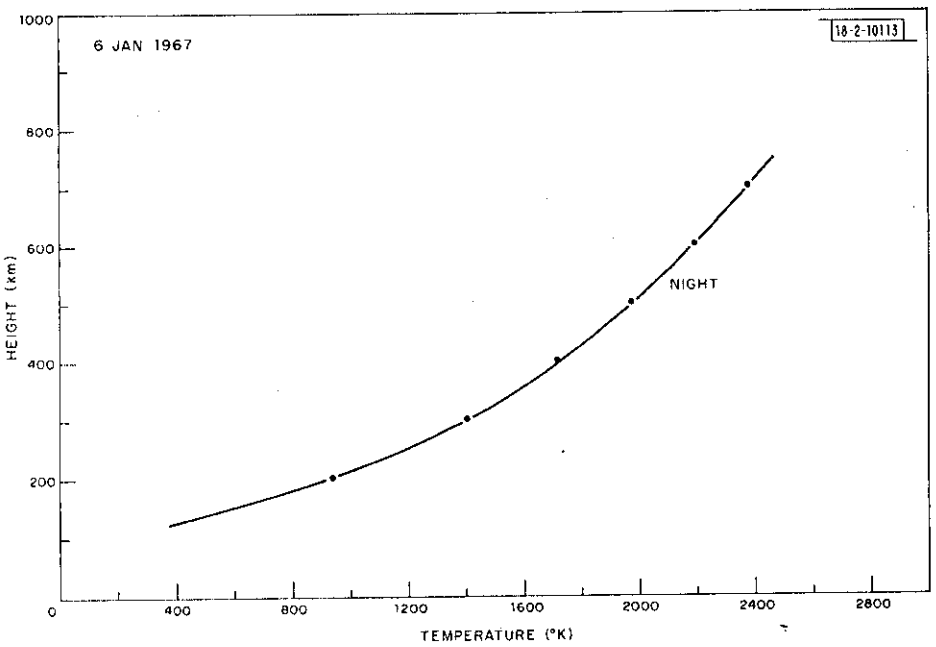

(a)

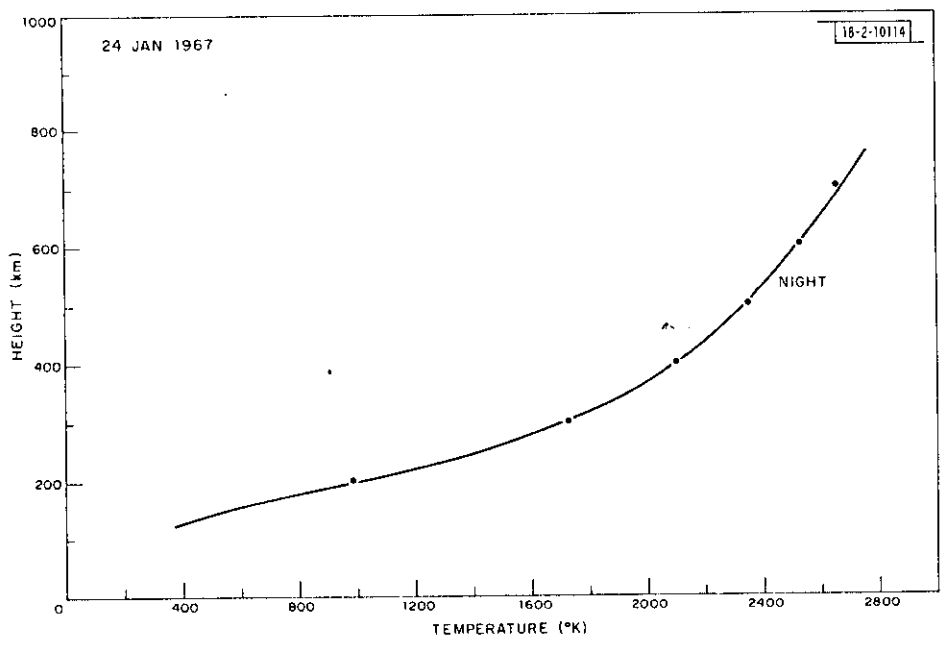

(b)

Fig. 7(a-z). Average variation of electron temperature during the daytime (1000 to 1500 EST) and nighttime (2100 to 0300 EST) for the observing periods.

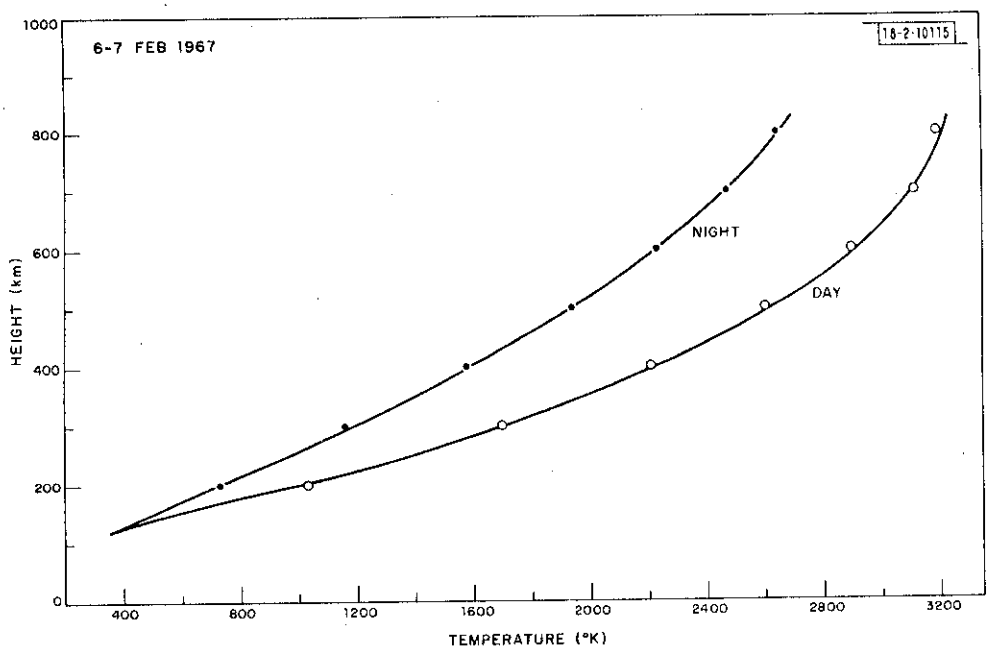

(c)

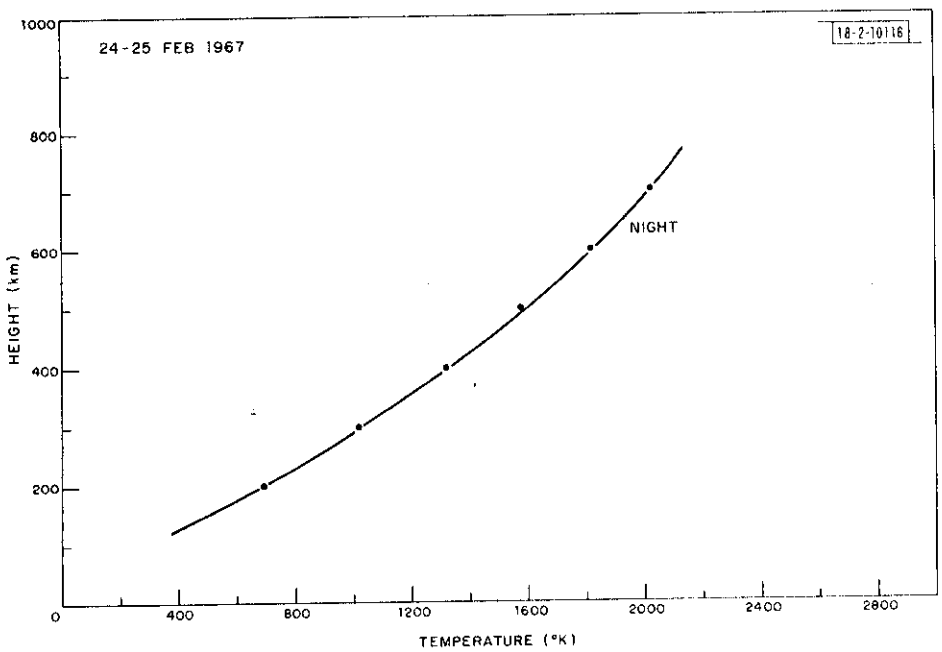

(d)

Fig. 7(a-z). Continued.

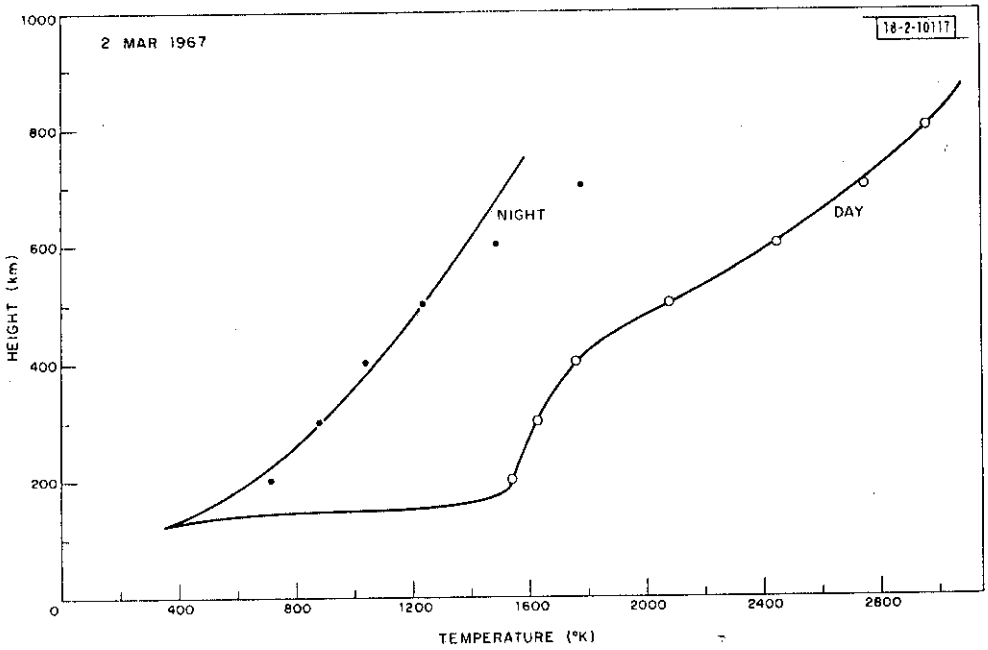

(e)

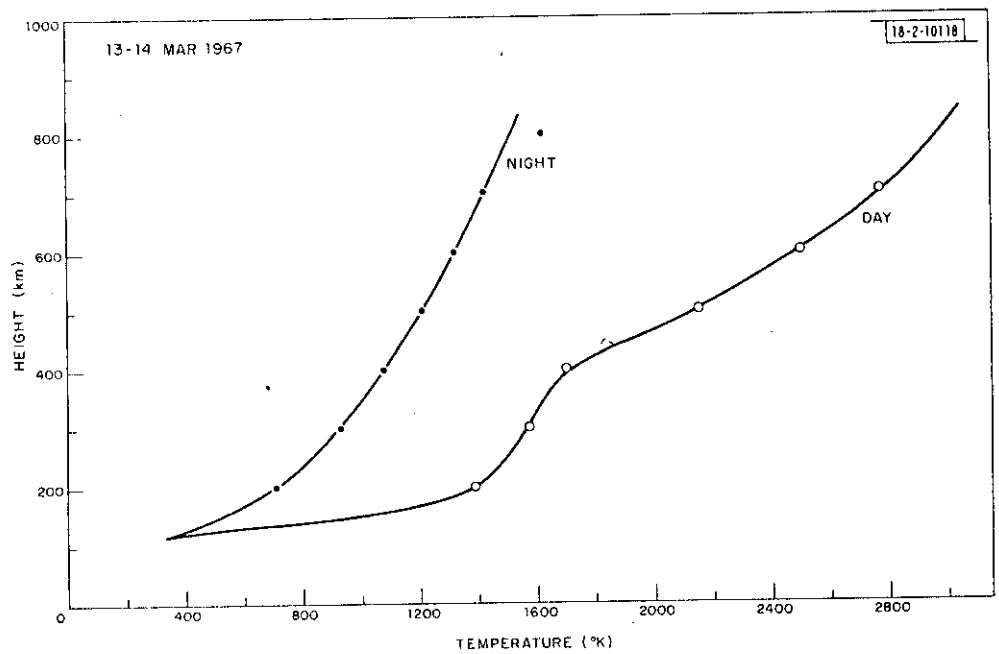

(f)

Fig. 7(a-z). Continued.

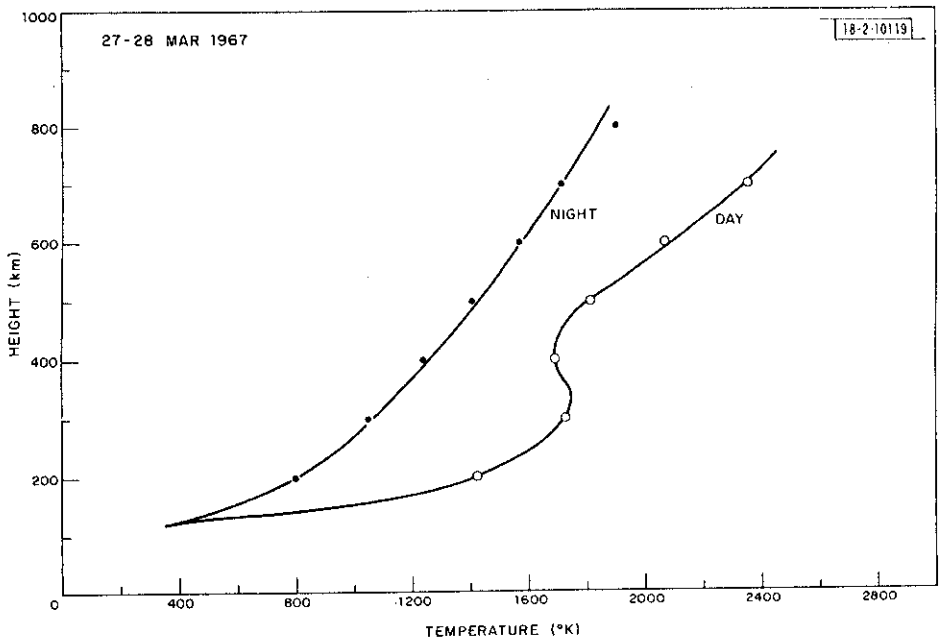

(g)

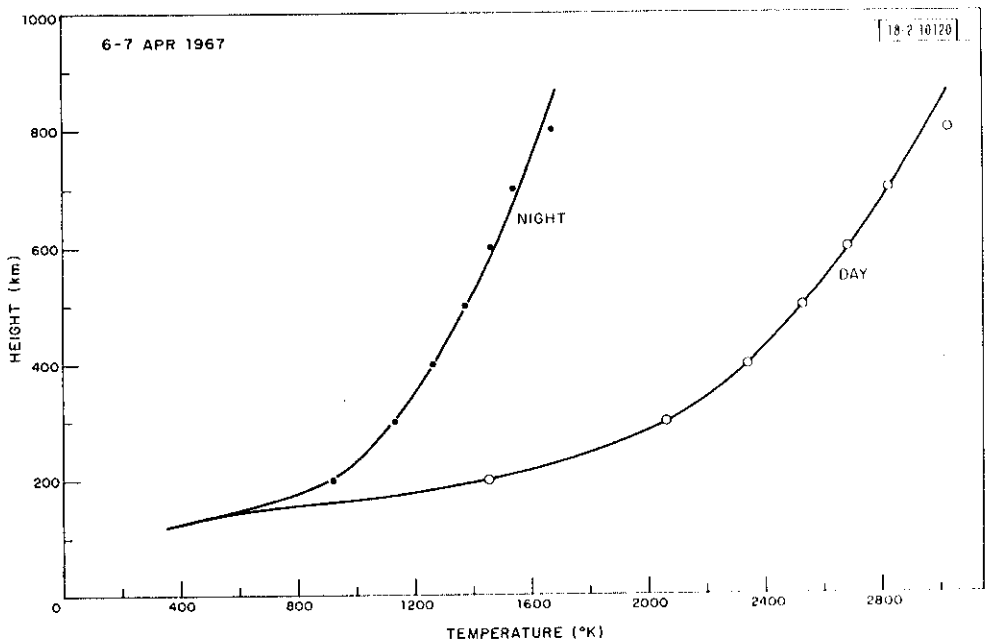

(h)

Fig. 7(a-z). Continued.

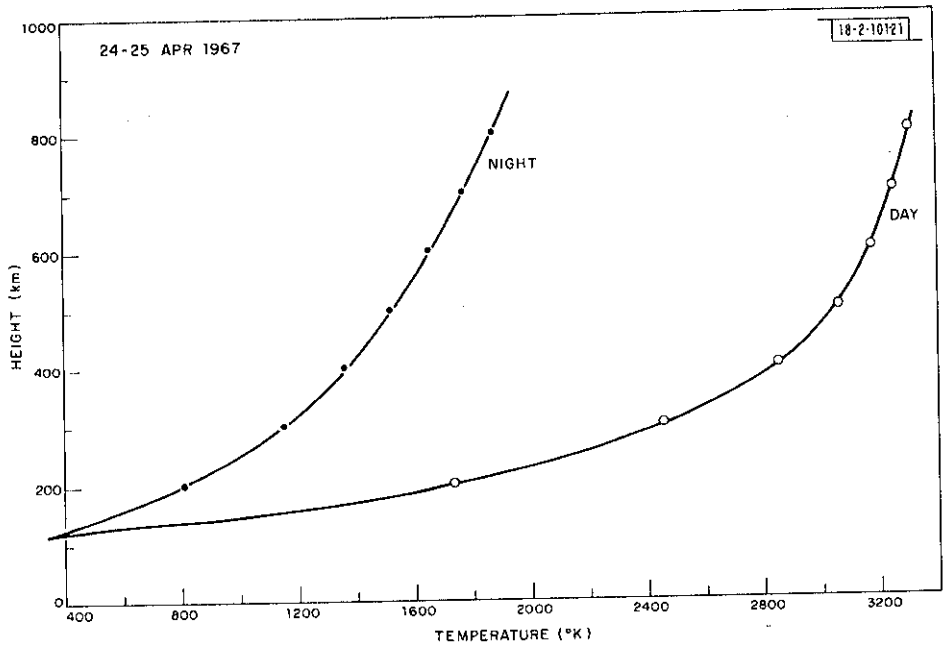

(i)

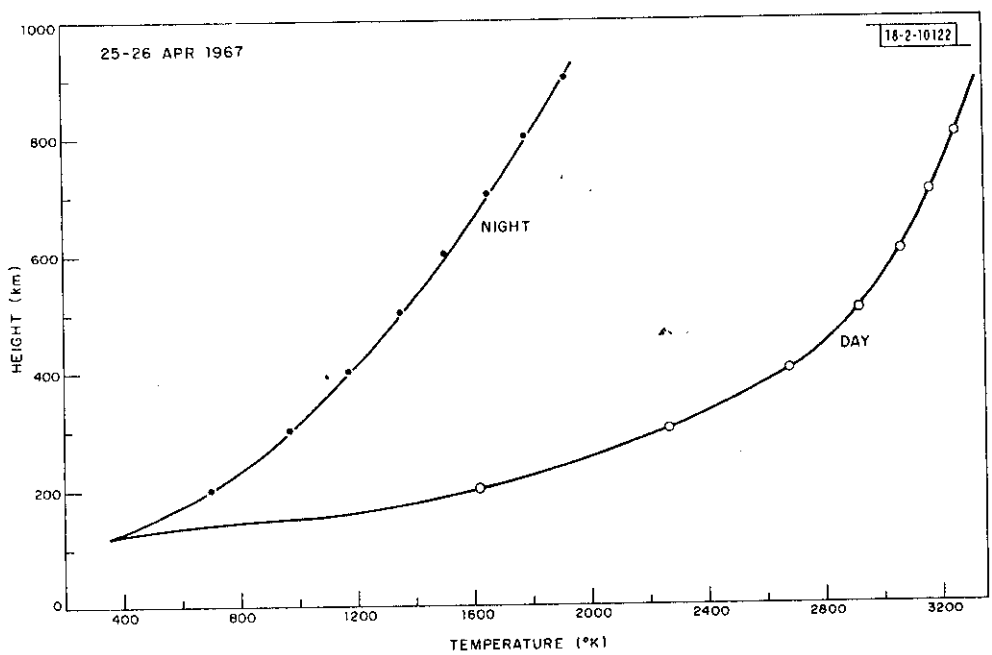

(j)

Fig. 7(a-z). Continued.

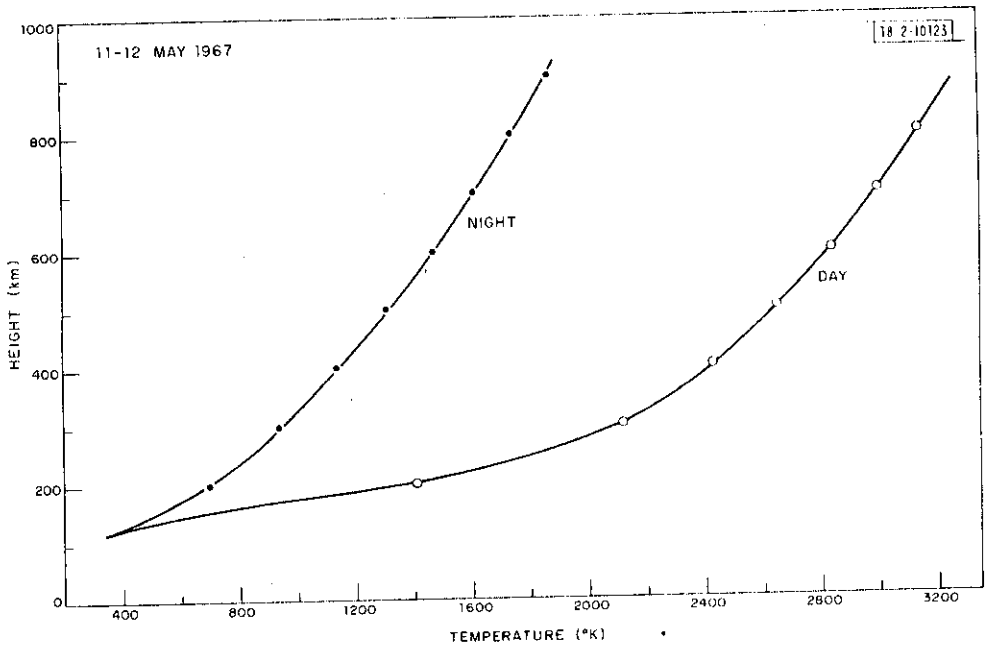

(k)

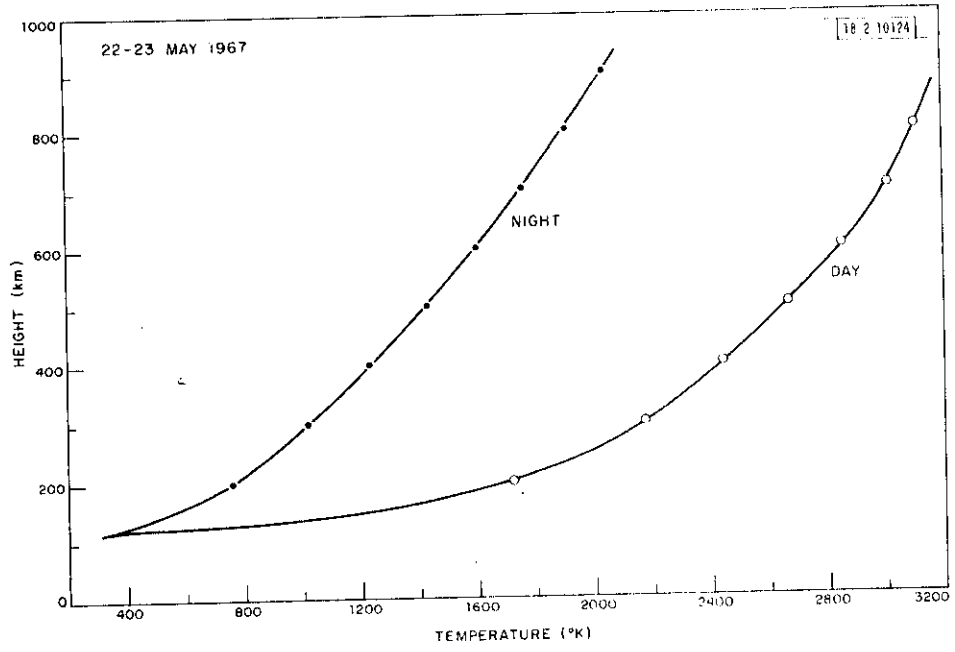

(l)

Fig. 7(a-z). Continued.

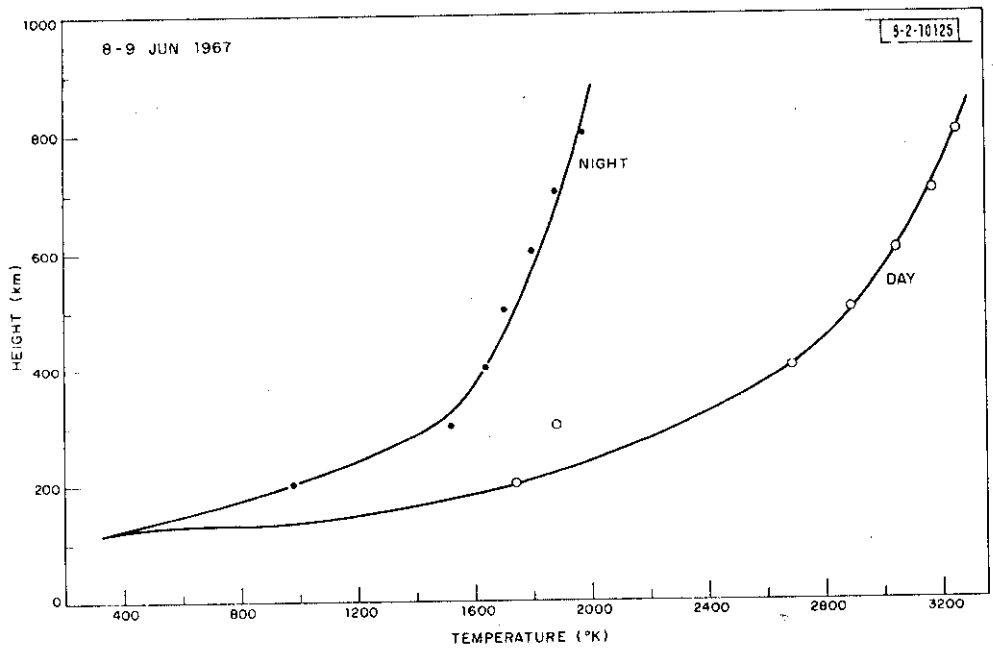

(m)

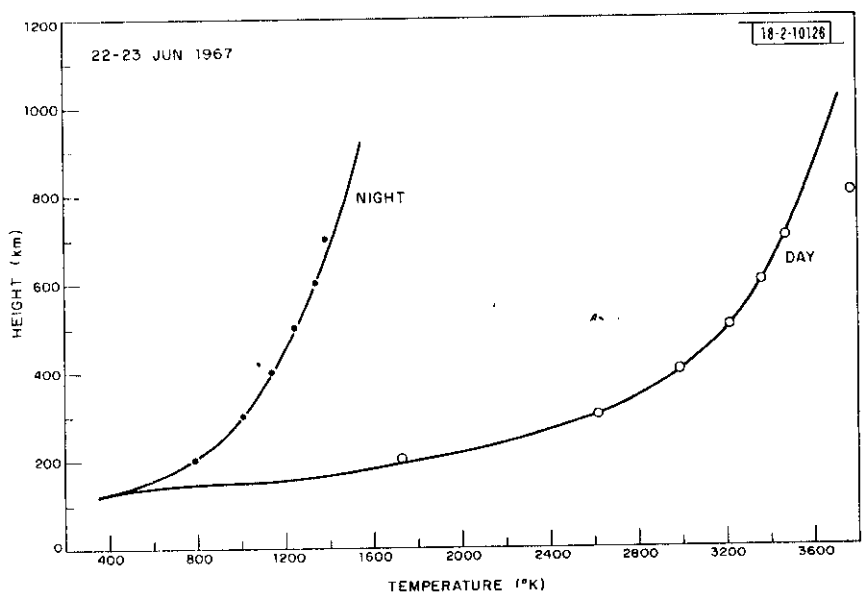

(n)

Fig. 7(a-z). Continued.

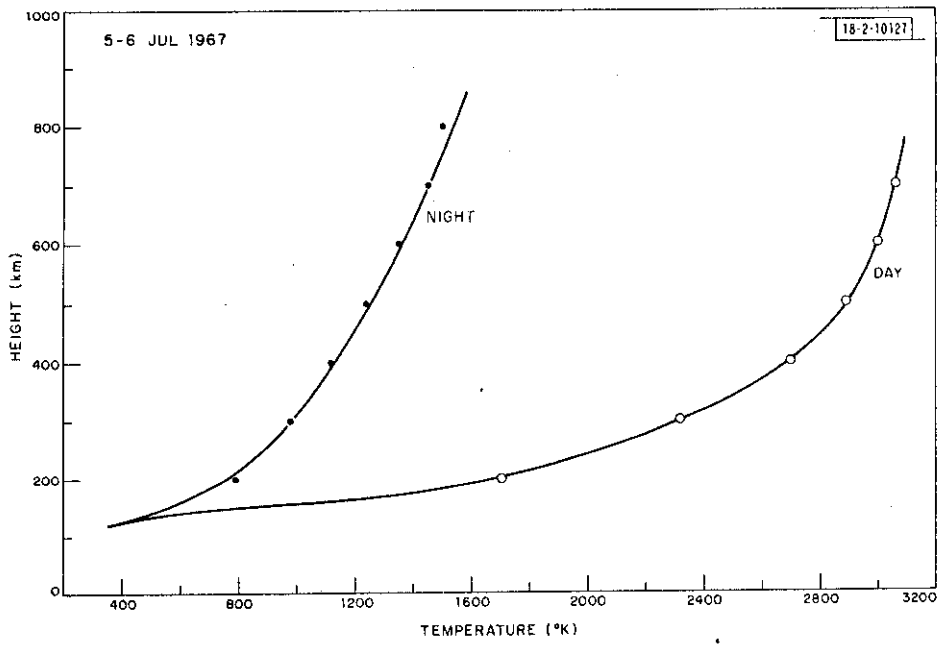

(o)

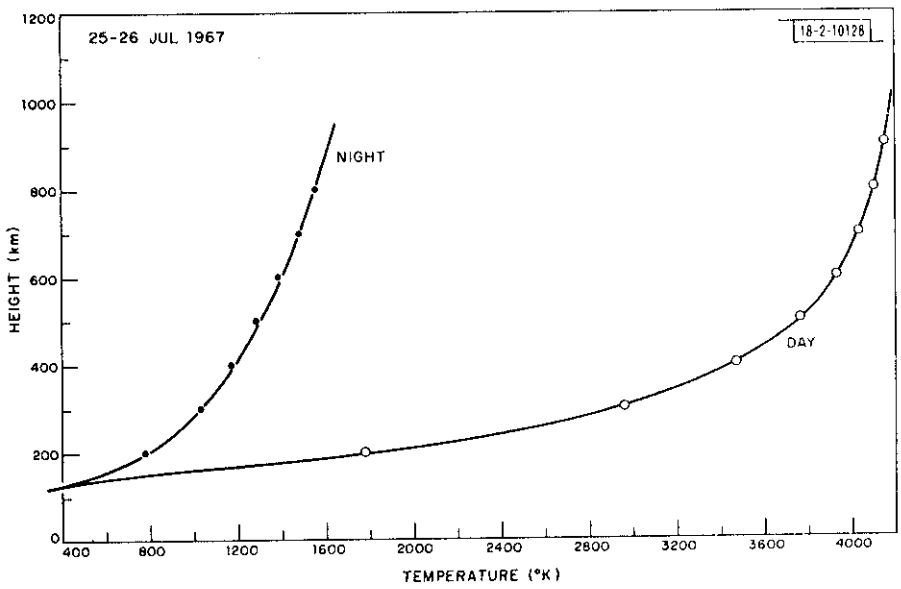

(p)

Fig. 7(a-z). Continued.

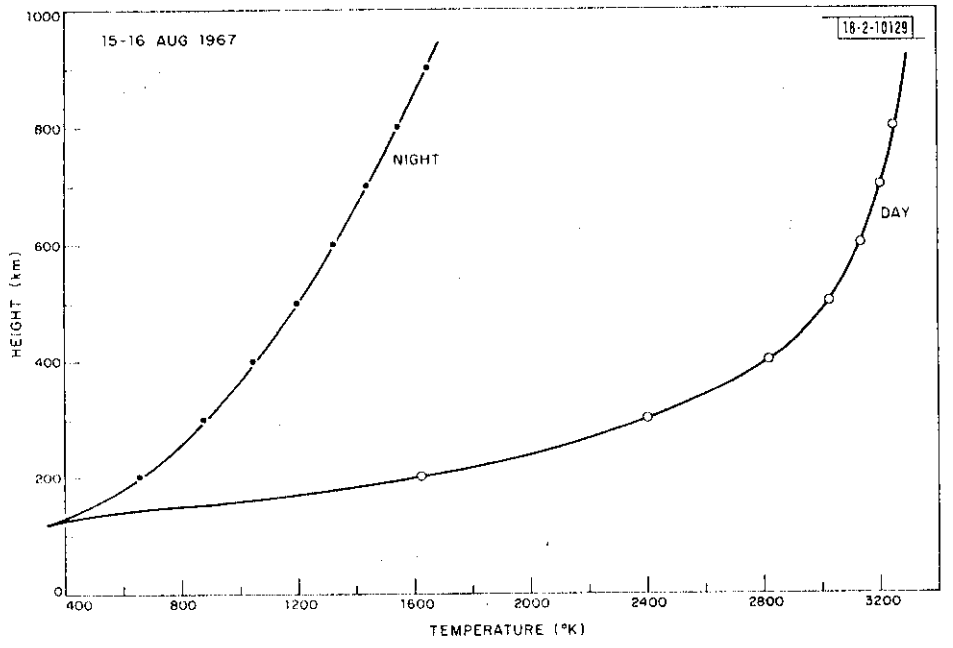

(q)

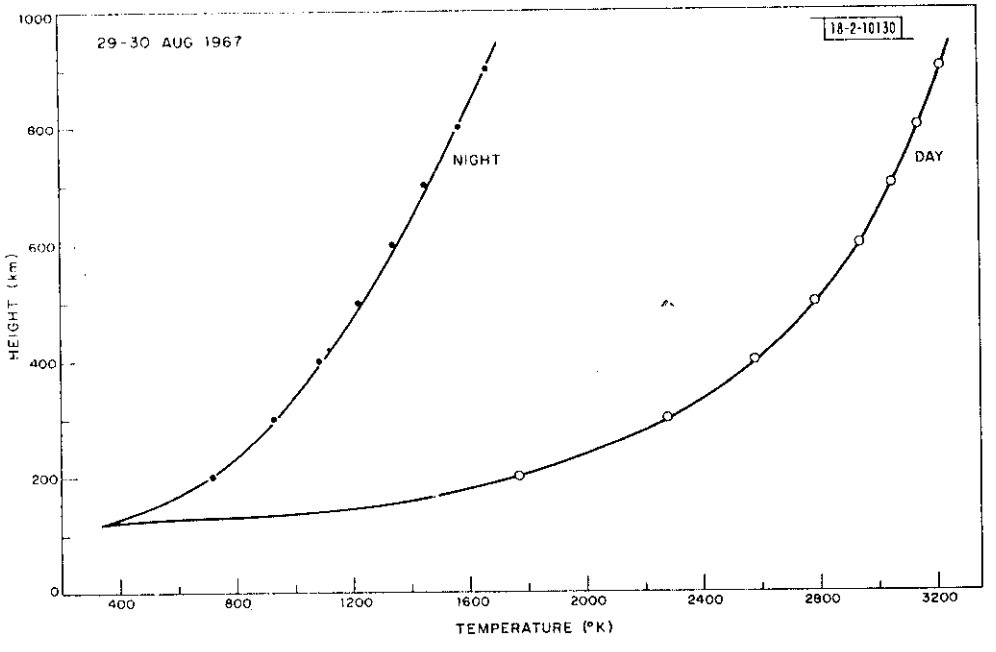

(r)

Fig. 7(a-z). Continued.

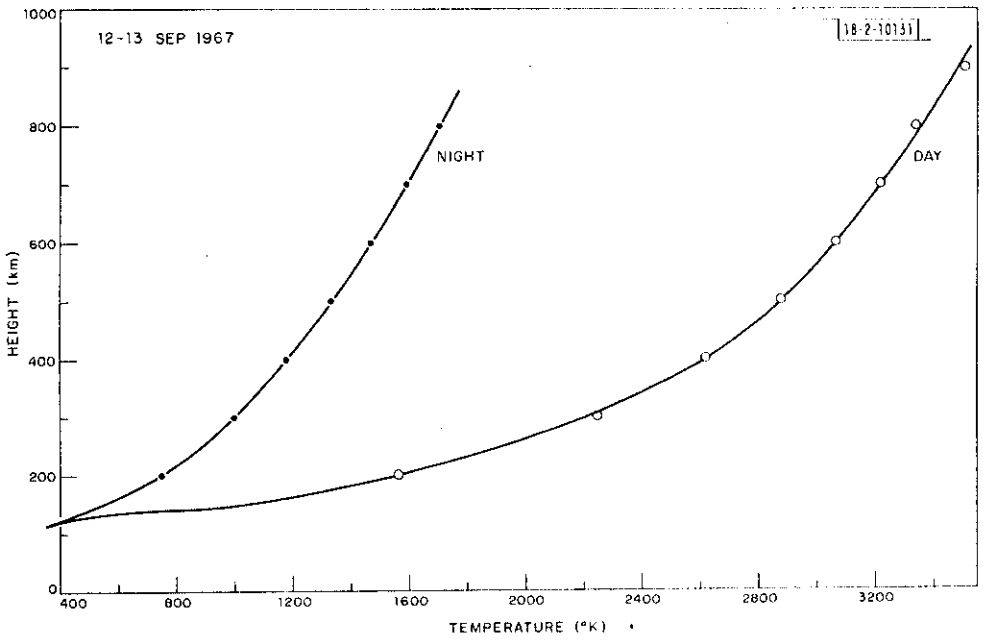

(s)

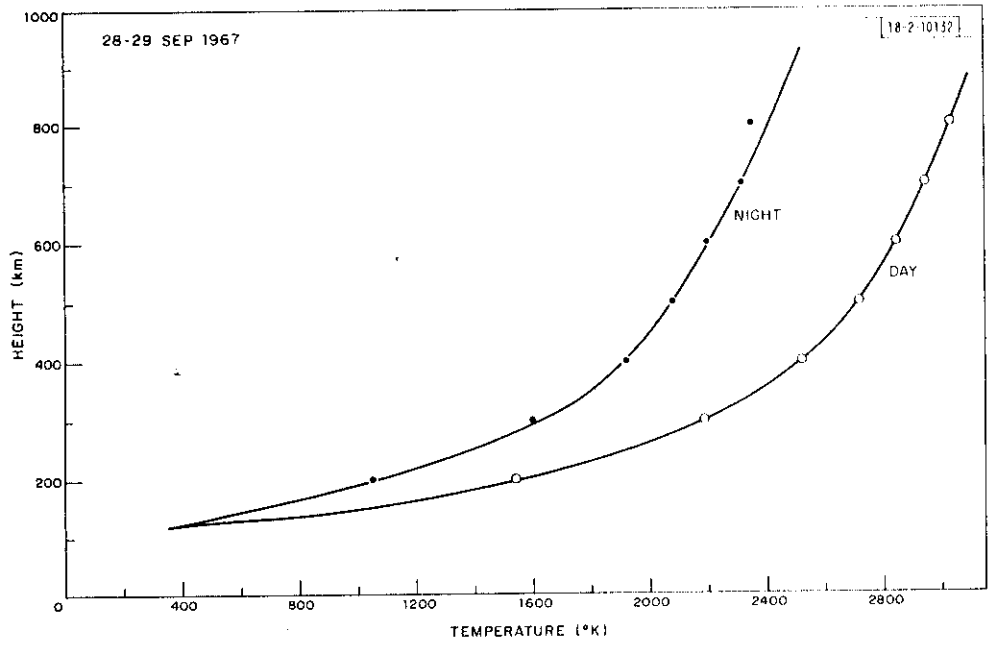

(t)

Fig. 7(a-z). Continued.

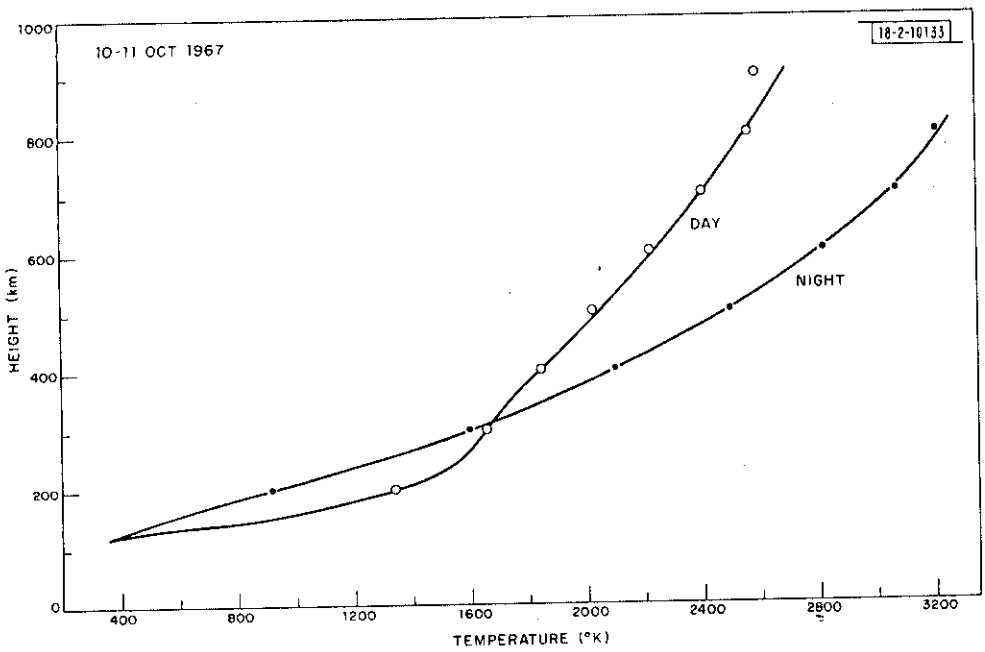

(u)

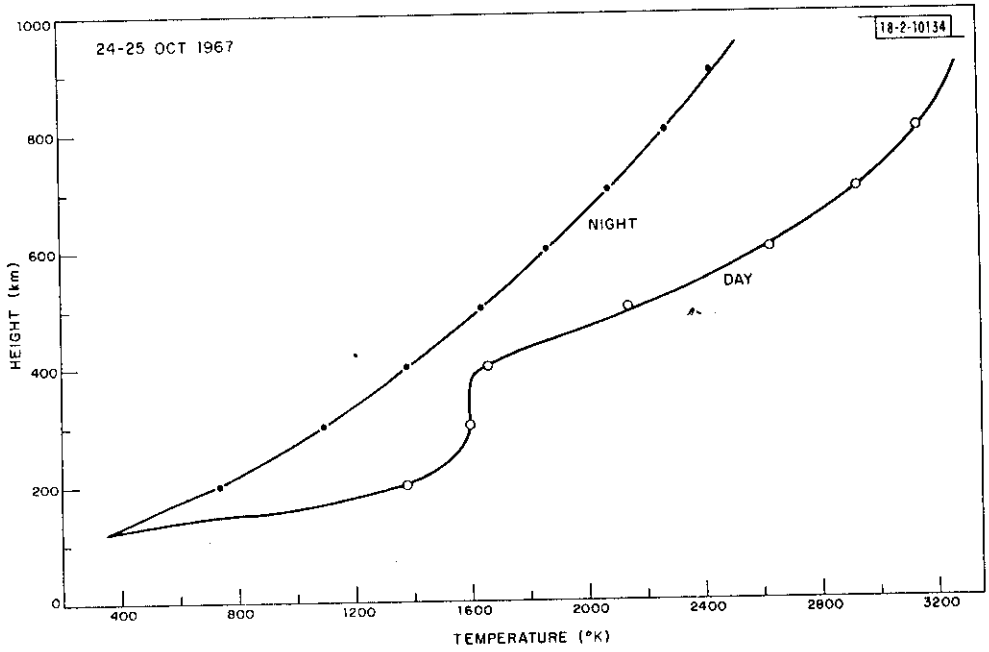

(v)

Fig. 7(a-z). Continued.

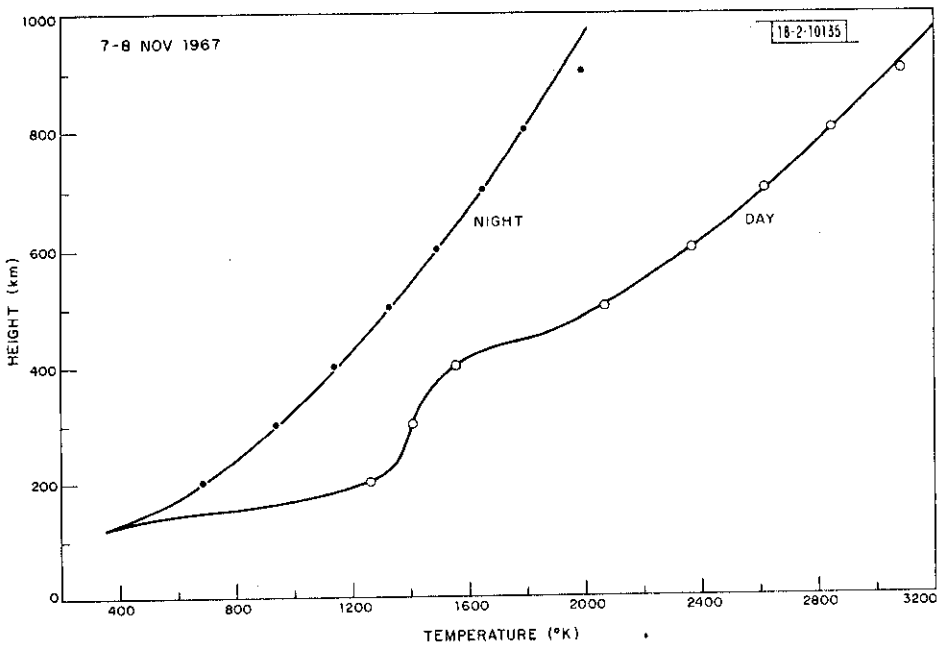

(w)

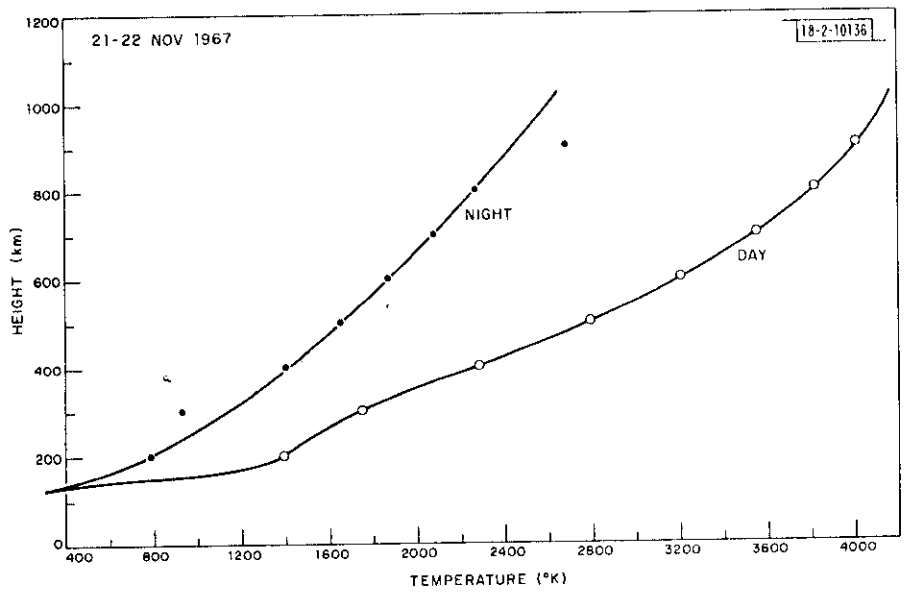

(x)

Fig. 7(a-z). Continued.

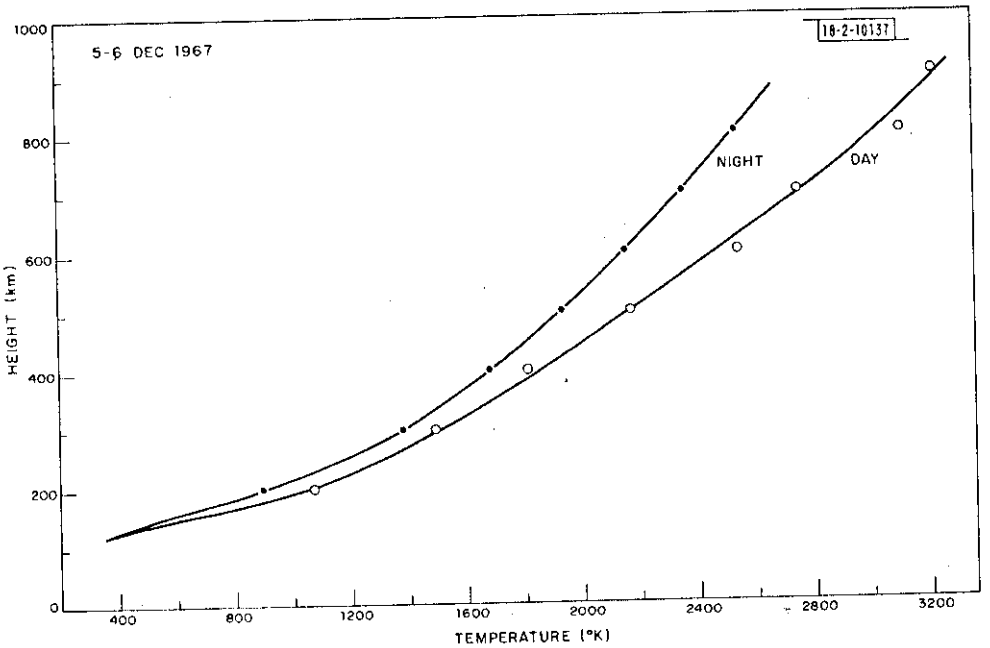

(y)

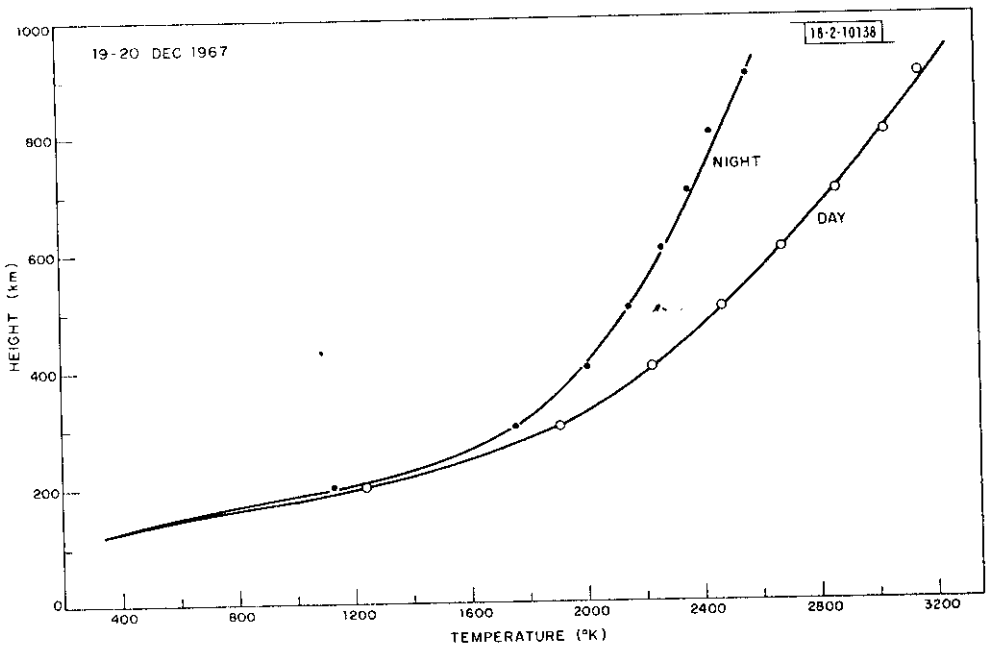

(z)

Fig. 7(a-z). Continued.

V. SEASONAL VARIATIONS

A. Electron Temperature

Figures 8(a) and (b) present the seasonal variation of the average temperatures in the form of contour diagrams of constant temperature vs height and date. The contours are at intervals of 500°K and show clearly that the daytime temperatures are higher in summer and the nighttime temperatures are higher in winter.

Figures 9(a) and (b) show the variation of the average T_e values [Figs. 7(a) through (z)] at 300 and 500 km vs date for the daytime and nighttime. These figures show somewhat more clearly the seasonal variation in T_e with peak daytime values in summer (April to September) and low values in winter (October to March). The plot for the nighttime variation [Fig. 9(b)] shows clearly the instances of nocturnal heating, the most pronounced of which appear to have occurred on 8-9 June, 28-29 September and 10-11 October.

B. Protonospheric Heat Flux

We have computed the average heat flux G_p entering the ionosphere from the magnetosphere along lines of force from the observed electron temperature gradient dT_e/dh and temperature T_e through

$$G_p = 7.7 \times 10^5 T_e^{5/2} \frac{dT_e}{dh} \sin^2 I \text{ eV/cm}^2\text{/sec} \qquad (3)$$

where I is the dip angle of the earth's magnetic field. The temperature curves employed for this calculation were the average temperature plots of Figs. 7(a) through (z). The temperature gradient dT_e/dh was estimated for each 100-km interval above 500-km altitude from simple differences, and the temperature at the center of each 100-km interval was taken as the appropriate value of T_e in Eq. (3). These independent estimates of G_p were then averaged and are plotted for the daytime and nighttime periods in Figs. 10(a) and (b).

It can be seen that most of the daytime values [Fig. 10(a)] lie in the range 4 to 7×10^9 eV/cm^2/sec, i.e., somewhat larger than the average values observed in previous years.[4,11,19] It is not clear whether this is a sunspot cycle effect. To test this we have listed in Table VII the values of the average heat flux for the winter period (October to March) and summer period (April to September) vs date. It is clear that the winter values exceed the summer values in all years and that there appears to be a slight trend of increasing flux toward sunspot maximum. A greater trend may exist but be masked by differences in the method employed to estimate G_p from year to year.

We have suggested elsewhere[4] that these daytime heat fluxes are close to the value for the total amount of energy escaping from the ionosphere above Millstone in the form of photoelectrons. Thus a variation with sunspot cycle can be understood in terms of a change in the solar EUV flux. However, a summer to winter difference cannot be attributed to this cause. Earlier,[19] we speculated that the seasonal variation in the heat flux was caused by a reduction in the number of escaping photoelectrons in summer due to the production of a greater number of electrons with pitch angles near 90° (Ref. 20). However, more recent studies of photoelectron escape[21,22] suggest that elastic scattering will rapidly alter the initial pitch angle distribution so that this phenomenon should be unimportant. Thus a more plausible explanation may depend upon the change in the neutral composition with season.[14]

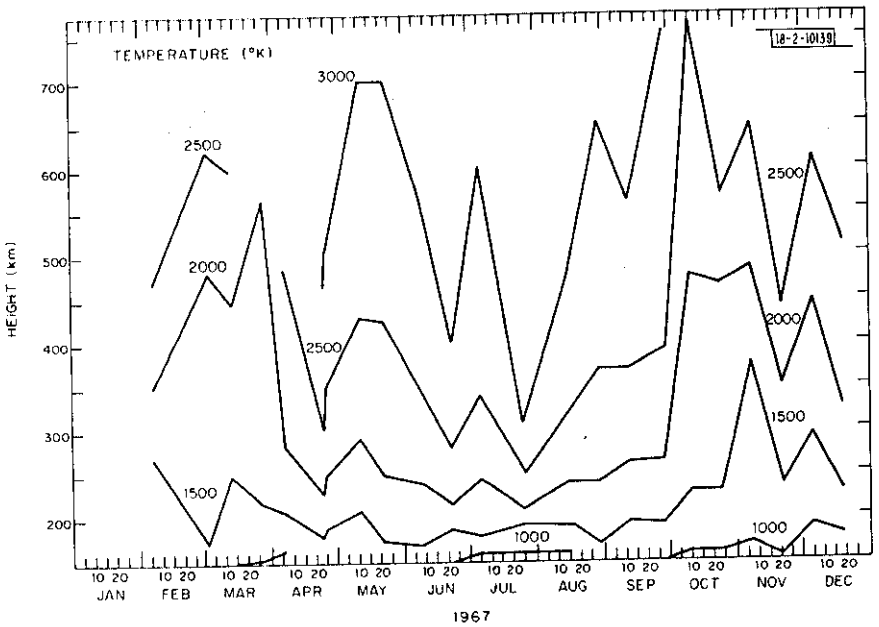

(a) Daytime (1000 to 1500 EST).

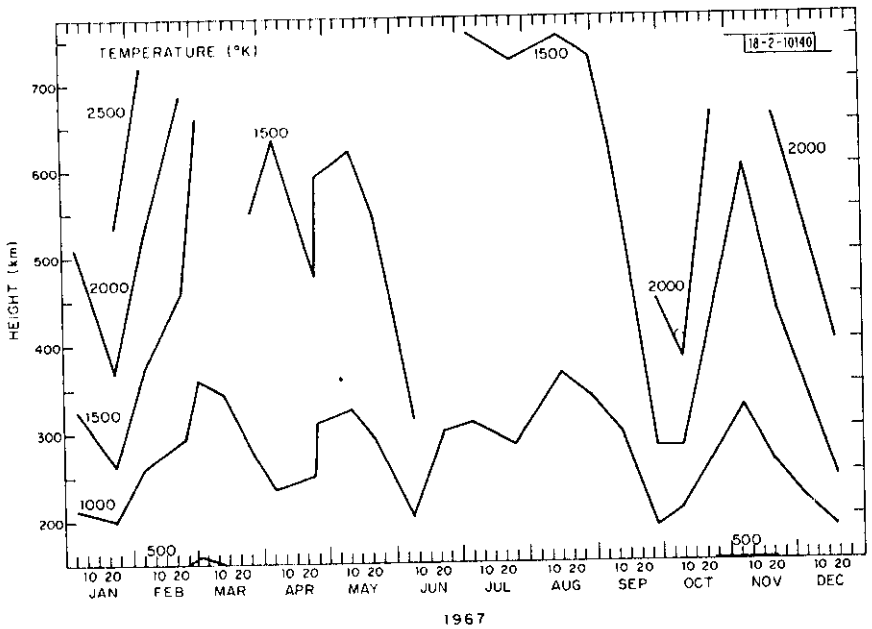

(b) Nighttime (2100 to 0300 EST).

Fig. 8. Contour plots, at 500°K intervals, of average electron temperature (°K) vs height and date taken from the temperature profiles of Figs. 7(a) through (z).

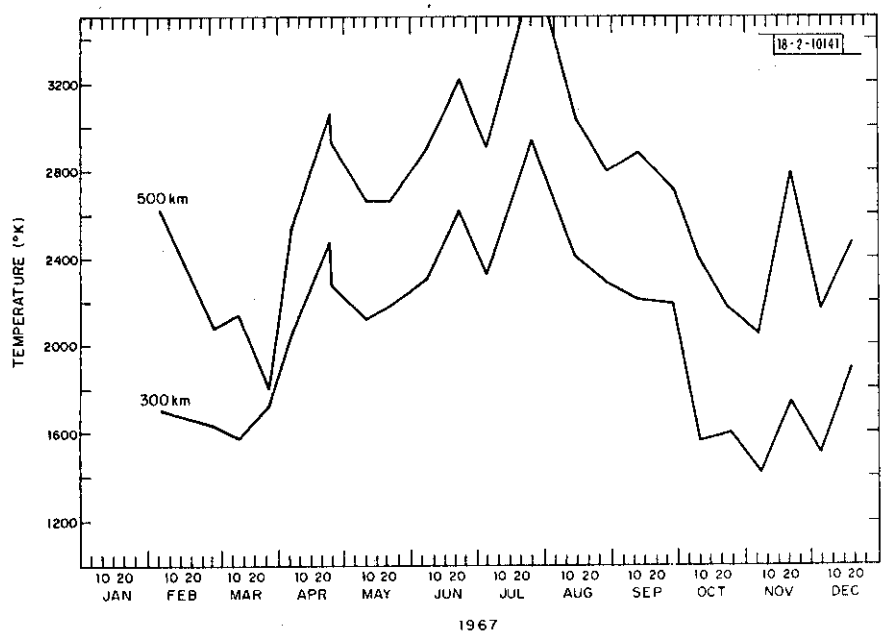

(a) Daytime (1000 to 1500 EST).

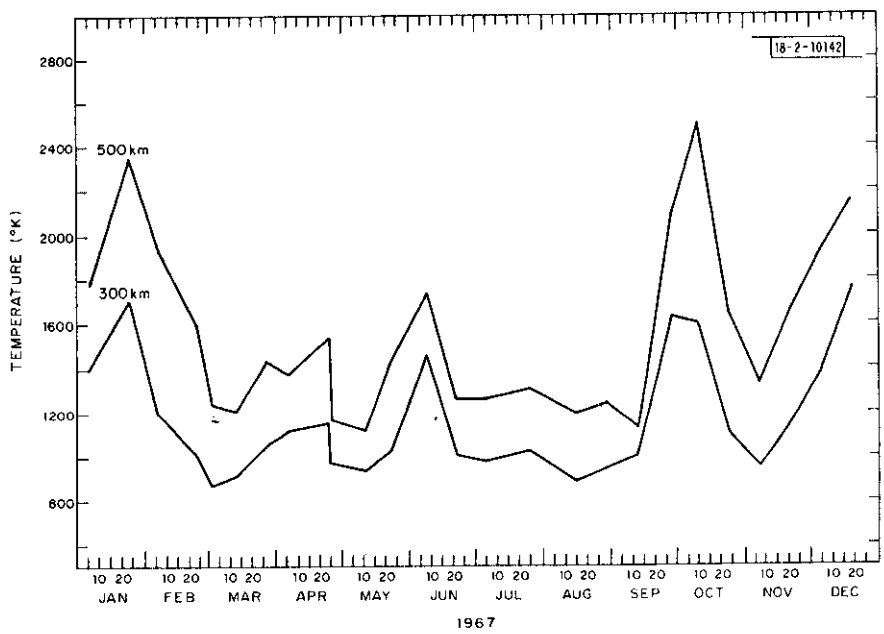

(b) Nighttime (2100 to 0300 EST).

Fig. 9. Variation of electron temperature at 300 and 500 km vs date taken from the average electron temperature profiles [Figs. 7(a) through (z)].

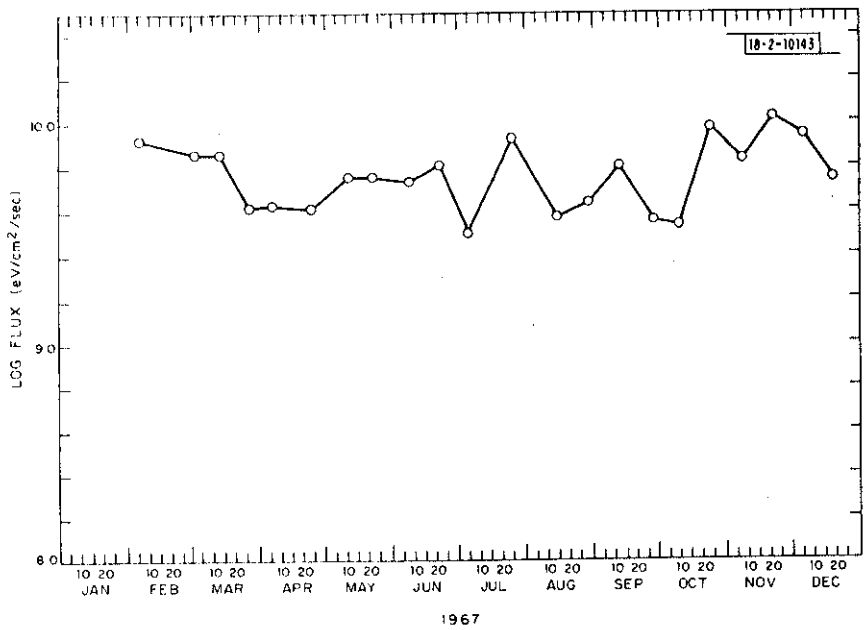

(a) Daytime (1000 to 1500 EST).

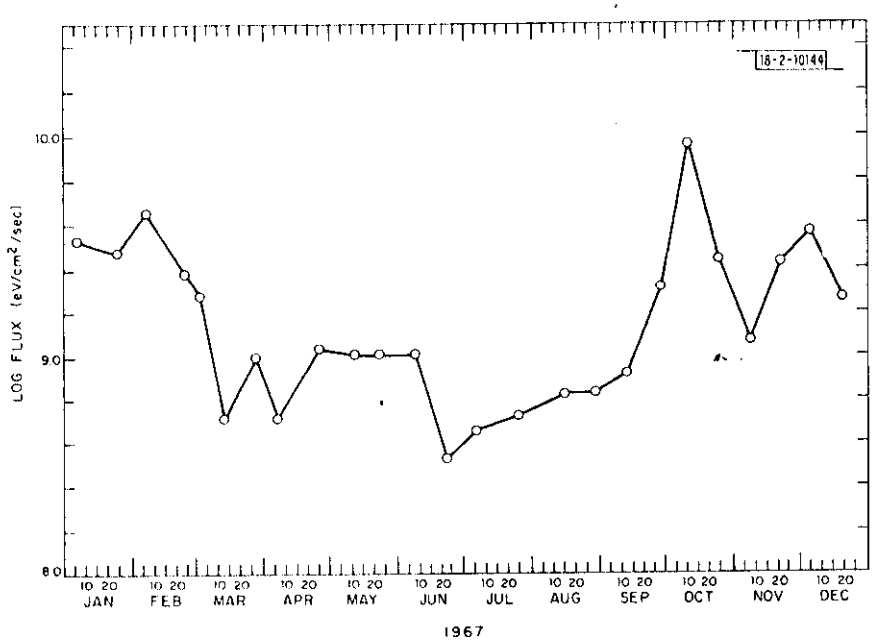

(b) Nighttime (2100 to 0300 EST).

Fig. 10. Variation of protonospheric heat flux vs date computed from the average electron temperature profiles [Figs. 7(a) through (z)].

TABLE VII

RESULTS FOR THE DAYTIME HEAT FLUX FROM THE PROTONOSPHERE

Year	Average Heat Flux (10^9 eV/cm^2/sec)		Ref.	Comment
	Winter	Summer		
1964	5.2	3.7	19	Computed for 500-km altitude
1965	3.2	2.0	11	Computed for 600-km altitude
1966	4.4	3.7	4	Average through 500- to 600-, 600- to 700- and 700- to 800-km intervals
1967	7.7	5.1	This paper	As for 1966

The nighttime values of the heat flux [Fig. 10(b)] show a pronounced seasonal variation with summer nighttime values 5 to 10 times lower than the daytime values, but winter nighttime values only a factor of two lower than the daytime values. As already noted, this can be attributed to conjugate point heating of the protonosphere during winter nights. Particularly striking in Fig. 10(b) is the large heat input on 10-11 October when G_p exceeds its daytime value. Clearly an additional source of heating of the protonosphere is required to explain such an event. As outlined above, we believe that energy injected in the form of ring current protons is the principal source.

VI. SUMMARY

We have presented results obtained for the F-region electron density and temperature at Millstone Hill during 1967. This was the last year in which all the spectra of the signals (from which the results for electron and ion temperature are obtained) were recovered in non-real-time from magnetic tape recordings of the IF signals. This scheme was abandoned in 1968 in favor of real-time spectrum analysis employing computer integration of the samples.[16] The spectrum analyzer employed during 1967 distorted the echo power spectra in a way which made the estimation of ion temperature somewhat unreliable[3] and these data have not been included in this report.

The measurements conducted in 1967 (Table II) achieved a time resolution of 30 minutes for a complete profile of electron density and temperature and were made twice per month for periods of 24 hours at a time. This program yielded over 1000 profiles of electron density and temperature. To present these in a manageable form, we have constructed contour diagrams of constant density [Figs. 5(a) through (x)] and temperature [Figs. 6(a) through (w)] vs height and time for each observing period.

These contour diagrams display a rich variety of different types of behavior. Geomagnetically quiet days tended to follow patterns recognized earlier. Thus, in winter there is typically a marked diurnal variation in the electron density with a peak near noon and often a smaller secondary maximum in the early morning (0200 to 0400 EST). In summer, by contrast, the layer shows a smaller diurnal variation and reaches a peak near ground sunset. Typically $h_{max}F2$ is higher in summer than winter and the "thickness" of the F-layer is larger also.

Some magnetically disturbed days also followed a distinct pattern noted earlier.[10] On the first day of the storm, N_{max} and h_{max} were normal until the afternoon when they both increased to very high values. There was a corresponding decrease in electron temperature. During the night T_e remained high, providing evidence of nocturnal heating and the following morning N_{max} and h_{max} were low and T_e very high.

As a rule, anomalous behavior of the electron density was accompanied by anomalous temperature variations, high values of T_e being associated with low values of density and vice versa. On some occasions the F-region density fell to extremely low values, suggesting that the trough region of low density associated with the plasmapause had moved south to occupy a position over Millstone. Electron temperature rose to particularly high values on these occasions. Toward the end of 1967, low latitude auroral activity appears to have been present on some nights with the result that auroral returns were detected at Millstone as oblique echoes at ~600-km range.

The average electron temperature variation with altitude has been constructed for a daytime period (1000 to 1500 EST) and a nighttime period (2100 to 0300 EST). These curves show that there was a seasonal variation of T_e, both by day and by night. The summer daytime values are higher than those in winter and we believe that this is simply a consequence of the seasonal variation in electron density. The reverse behavior is found at night and is caused by nocturnal heating of the ionosphere in winter by the protonosphere. This is warmed by photoelectrons escaping from the conjugate region which remains sunlit.

From the average daytime electron temperature curves we have computed the heat flux from the protonosphere and compared this with that observed in previous years (Table VII). The average values for 1967 appear higher than in 1966 and 1965 suggesting a sunspot cycle variation. We find also a consistent seasonal variation with the summer values averaging 2/3 of the winter ones. The reason for this is not understood but may stem from the change in the neutral composition that is believed to occur in the thermosphere.[14]

ACKNOWLEDGMENTS

W. Abel and W.A. Reid were largely responsible for collecting these data. They were assisted by J.H. McNally, A. Beauregard and others of the staff of the Millstone Hill Observatory. The author would also like to acknowledge the efforts of R. Julian, J.K. Upham, Mrs. A. Freeman and Miss L. Zak in various portions of the data analysis. The continued support of P.B. Sebring is also gratefully acknowledged.

REFERENCES

1. J.V. Evans, "Ionospheric Backscatter Observations at Millstone Hill," Technical Report 374, Lincoln Laboratory, M.I.T. (22 January 1965), DDC AD-616607.
2. _____, "Millstone Hill Thomson Scatter Results for 1964," Technical Report 430, Lincoln Laboratory, M.I.T. (15 November 1967), DDC AD-668436.
3. _____, "Millstone Hill Thomson Scatter Results for 1965," Technical Report 474, Lincoln Laboratory, M.I.T. (18 December 1969), DDC AD-707501.
4. _____, "Millstone Hill Thomson Scatter Results for 1966," Technical Report 481, Lincoln Laboratory, M.I.T. (15 December 1970), DDC AD-725742.
5. _____, Planet. Space Sci. 13, 1031 (1965), DDC AD-616607.
6. _____, J. Geophys. Res. 70, 1175 (1965), DDC AD-614310.
7. _____, Planet. Space Sci. 15, 1387 (1967).
8. _____, J. Geophys. Res. 75, 4803 (1970), DDC AD-714447.
9. _____, J. Geophys. Res. 75, 4815 (1970), DDC AD-714446.
10. _____, J. Atmos. Terr. Phys. 32, 1629 (1970), DDC AD-716057.
11. _____, Planet. Space Sci. 18, 1225 (1970), DDC AD-716056.
12. _____, J. Geophys. Res. 72, 3343 (1967), DDC AD-658912.
13. _____, and L.P. Cox, J. Geophys. Res. 75, 159 (1970), DDC AD-703492.
14. L.P. Cox and J.V. Evans, J. Geophys. Res. 75, 6271 (1970), DDC AD-722911.
15. J.V. Evans, J. Geophys. Res. 73, 3489 (1968), DDC AD-673605.
16. _____, R.F. Julian and W.A. Reid, "Incoherent Scatter Measurements of F-Region Density, Temperatures, and Vertical Velocity at Millstone Hill," Technical Report 477, Lincoln Laboratory, M.I.T. (6 February 1970), DDC AD-706863.
17. G.P. Serbu and E.J.R. Maier, J. Geophys. Res. 71, 3755 (1966).
18. K.D. Cole, J. Geophys. Res. 70, 1689 (1965).
19. J.V. Evans, Planet. Space Sci. 15, 1557 (1967).
20. F. Mariani, J. Geophys. Res. 69, 556 (1965).
21. R.J. Cicerone and S.A. Bowhill, Radio Sci. 5, 49 (1970).
22. _____, Radio Sci. 6, in press (1971).

DOCUMENT CONTROL DATA – R&D

(Security classification of title, body of abstract and indexing annotation must be entered when the overall report is classified)

1. ORIGINATING ACTIVITY *(Corporate author)*
Lincoln Laboratory, M.I.T.

2a. REPORT SECURITY CLASSIFICATION
Unclassified

2b. GROUP
None

3. REPORT TITLE
Millstone Hill Thomson Scatter Results for 1967

4. DESCRIPTIVE NOTES *(Type of report and inclusive dates)*
Technical Report

5. AUTHOR(S) *(Last name, first name, initial)*
Evans, John V.

6. REPORT DATE	7a. TOTAL NO. OF PAGES	7b. NO. OF REFS
22 July 1971	64	22

8a. CONTRACT OR GRANT NO.	9a. ORIGINATOR'S REPORT NUMBER(S)
F19628-70-C-0230	Technical Report 482
b. PROJECT NO. 7X263304D215	9b. OTHER REPORT NO(S) *(Any other numbers that may be assigned this report)*
c.	ESD-TR-71-199
d.	

10. AVAILABILITY/LIMITATION NOTICES
Approved for public release; distribution unlimited.

11. SUPPLEMENTARY NOTES	12. SPONSORING MILITARY ACTIVITY
None	Office of the Chief of Research and Development, Department of the Army

13. ABSTRACT

This report summarizes results for the electron density distribution and electron temperature of the F-region obtained during 1967 using the Millstone Hill (42.6°N, 71.5°W) Thomson (incoherent) scatter radar system. These data, for the height interval of approximately 200 to 800 km, were gathered over 24-hour observing periods twice per calendar month. The time required to obtain a complete electron density and temperature profile over this height interval was 30 minutes.

The results show a far wider range of behavior than that encountered in previous years. This is attributed to the increase in magnetic activity as sunspot maximum is approached. On magnetically quiet days, the characteristic behavior observed previously for electron density manifests itself. Winter days exhibit a maximum at all levels near noon and a weaker maximum at the layer peak in the early morning (0200 to 0400 EST), while summer days exhibit a maximum near sunset and only a small day-to-night change in density near the layer peak. Two days exhibited a pattern of behavior, first noted in 1965, that appears characteristic of many storms. This consists of an increase in density on the afternoon of the first day of the storm followed by a marked decrease the next morning. Other days show instances of nocturnal heating and erratic behavior of the F-region electron density at night. We believe that on several occasions in 1967 the plasmapause boundary moved south of Millstone giving rise to a rapid fall in f_0F2 and to much of the irregular behavior observed at night.

14. KEY WORDS

Millstone radar
F-region
diurnal variations
electron density
ionospheric scatter
seasonal variations
temperature effects
spectrum analyzers

☆ U. S. GOVERNMENT PRINTING OFFICE: 1972—704-102/19